universität wien

MASTERARBEIT / MASTER'S THESIS

Titel der Masterarbeit / Title of the Master's Thesis

„Peptide nanotubes as templates for silica precipitation"

verfasst von / submitted by

Stefan Riedl BSc

angestrebter akademischer Grad / in partial fulfilment of the requirements for the degree of

Master of Science (MSc)

Wien, 2017 / Vienna 2017

Studienkennzahl lt. Studienblatt / degree programme code as it appears on the student record sheet:	A 066 863
Studienrichtung lt. Studienblatt / degree programme as it appears on the student record sheet:	Biological Chemistry
Betreut von / Supervisor:	Univ.-Prof. Dr. Christian Friedrich Wilhelm Becker

Abstract

Several peptides are known, which have the ability to spontaneously assemble into higher order structures, such as nanotubes. Peptide nanotubes (PNTs) have attracted considerable interest in biotechnology and found great use in several applications, including drug delivery and tissue engineering. Burgess *et al.* designed a toolkit of self-assembling PNTs, based on different coiled-coil sequences, with various oligomerization states. Here, two peptides of this toolkit were modified with a short peptide sequence, derived from silaffin proteins, to obtain additional functionality of these coiled-coil PNTs. Silaffins are a group of proteins, originally discovered in diatoms, which are known to possess the ability to precipitate silica from silicic acid under physiological conditions. Adding silaffin peptides to the solvent exposed surface of PNTs *via* selective sidechain modification should enable the deposition of silica around the PNTs, yielding silica covered nanotubes.

Pentamer and hexamer forming coiled-coil peptides were synthesized, containing either one or two silaffin sidechain modifications. A successful assembly into nanotubes could only be observed in the case of the unmodified pentamer. Co-assembling modified and unmodified peptides resulted in a loss of the ability to form nanotubes. Silica precipitations, with silaffin modified coiled-coil peptides, yielded mostly spherical particles as observed for silaffin peptides alone. Silica covered nanotubes could only be obtained by adding silaffin modified pentamer to already assembled PNTs. Furthermore, to shed light on the assembly of the modified peptides, a pentamer modified with Cy5 instead of the silaffin was synthesized and incorporated into PNTs.

Zusammenfassung

Eine Vielzahl an Peptiden ist bekannt, die die Fähigkeit besitzt sich spontan zu höher geordneten Strukturen, wie Nanoröhren, zusammenlagern. Peptid-Nanoröhren (PNTs) haben ein großes Interesse in der Biotechnologie geweckt, und haben Verwendung in verschiedensten Bereichen, einschließlich der Medikamentengabe oder dem Tissue Engineering, gefunden. Burgess *et al.* entwickelten ein Repertoire von selbst-assemblierenden PNTs, basierend auf Coiled-Coil Sequenzen, mit unterschiedlichen Oligomerisierungs-Zuständen. Um diese Coiled-Coil-PNTs weiter zu funktionalisieren, wurden zwei Peptide ausgewählt und mit einer kurzen Silaffin-Peptidsequenz modifiziert. Silaffine sind eine Gruppe von Proteinen, die ursprünglich in Kieselalgen entdeckt wurde und die Fähigkeit besitzen, Siliziumdioxid aus Kieselsäure unter physiologischen Bedingungen zu präzipitieren. Im Rahmen dieser Arbeit wurden selektiv kurze Silaffin-Sequenzen auf der Lösungsmittel-exponierten Oberfläche von Peptid-Nanoröhrchen angebracht. Dies sollte zur Präzipitation von Siliziumdioxid um die PNTs führen, wodurch Siliziumdioxid ummantelte Nanoröhrchen entstehen.

Um den Effekt der eingeführten Modifikation auf die Nanoröhrchen zu untersuchen, wurden Pentamere und Hexamere aus dem Coiled-Coil-Toolkit synthetisiert, die entweder eine oder zwei Silaffin-Modifikationen an Aminosäureseitenketten enthielten. Eine erfolgreiche Assemblierung zu Nanoröhren konnte jedoch nur im Falle des unmodifizierten Pentamers beobachtet werden. Die Ko-Assemblierung von modifizierten und unmodifizierten Peptiden führte ebenfalls zu einem Verlust der Fähigkeit Nanoröhrchen zu bilden. Präzipitationen mit den modifizierten Coiled-Coil Peptiden resultierten hauptsächlich in sphärischen Partikeln, wie sie auch mit Silaffinen alleine beobachtet werden. Siliziumdioxid-Nanoröhren konnten jedoch erfolgreich erhalten werden, indem bereits assemblierte PNTs aus unmodifizierten Pentamer mit modifizierten Peptid kombiniert wurden. Um darüber hinaus die Assemblierung der modifizierten Peptide zu studieren, wurde eine Version des Pentamers mit Cy5 anstelle der Silaffin Modifikation synthetisiert.

Table of contents

1 Introduction

1.1 The coiled-coil motif in proteins

The coiled-coil is an abundant structural motif in proteins. Around 6% of proteins contain structural elements in their sequence, which can be assigned as coiled-coil domains. Over 6000 proteins containing possible coiled-coil motifs were already identified in GenBank by Odgren and coworkers. [1] The motif itself was first described by Francis Crick in 1953. He characterized the coiled-coil as a sense pack of α-helices, which are around 20 ° away from parallel, thus wrapping around each other. [2] Most common are coils consisting out of two or three helices. However, coiled-coils with up to seven helices have been found. [3] At about the same time as Francis Crick, Linus Pauling proposed the coiled-coil motif as a model for α-keratin. [4] These intermediate filaments can be found in hairs, nails or feathers and provide stability for many biological structures. Coiled-coils got even more attention, when it was discovered, that they play a crucial role in important transcription mechanisms. A famous example for that is GCN4, which has a dimeric leucine zipper motif. The leucine zipper interacts directly with DNA and allows the protein to act as a transcription factor. [5] Coiled-coils also play an important role during infection of T-cells with HIV. Gp41, a coiled-coil glycoprotein consisting of six helices, and gp120 are mainly responsible for the fusion of the membranes during viral entry. [6] Due to their highly specific interactions, coiled-coils also found use as dimerization tags for various applications. [7]

The most abundant form of coiled-coils is left-handed and exhibits a heptad repeat of amino acids in their sequence. These repeats can range up to over 200 in some proteins and are denoted with the letters **a-b-c-d-e-f-g**. [8] The seemingly simplicity of the heptad structure was extensively studied and led to several hypotheses describing the necessary elements in the repeat. O'Shea *et al.* used the "Peptide Velcro" (PV) hypothesis to describe the design strategies for the formation of dimeric coiled-coils. This hypothesis states, that in principal only three structural elements are required for coiled-coils (Fig. 1-1). [9]

Firstly, the **a** and **d** position of the repeat must contain hydrophobic amino acids. Having nonpolar amino acids at these positions facilitates the dimerization by stabilizing van der Waals interactions along the face of each helix. Crick already described this in 1953, when he proposed a "knobs-into-holes" packing style of the hydrophobic side chains. [2] The hydrophobic amino acids can also play a crucial role in defining the oligomerization state of the coils. In the dimeric GCN4 leucine-zipper a valine occurs at the **a** position, while

leucine can be found in the **d** position. [10] The replacement of valine with leucine and leucine with isoleucine resulted in a tetrameric coiled-coil. [11] Only valines lead to a mixture of dimers and trimers, whereas leucine at both position resulted also in a tetrameric coil.

In general, a high percentage of a hydrophobic amino acids at the **a** and **d** position leads to more stable coiled-coils. [12] Therefore, the use of non-natural amino-acids, which are more hydrophobic than the natural ones, such as 5,5,5-trifluoroleucine, led to a further increase in the stability of the coiled-coils. [13]

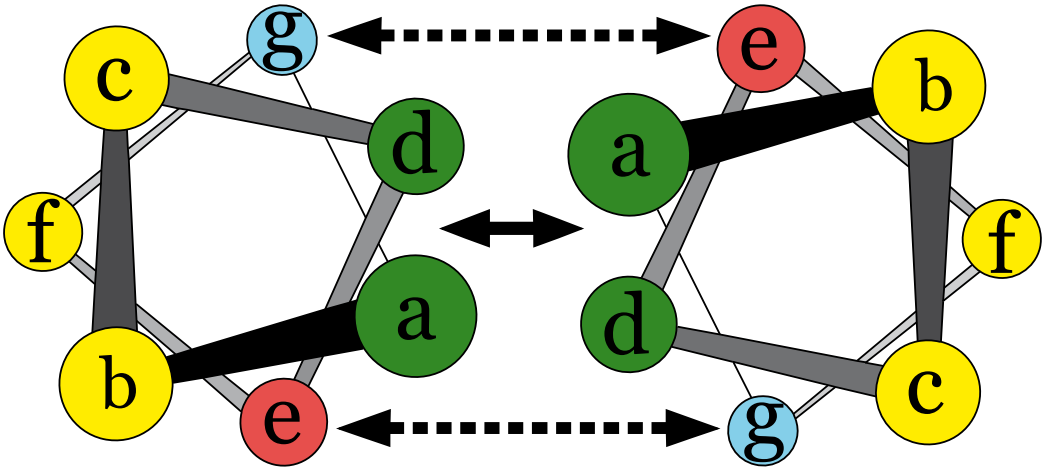

Figure 1-1 Schematic illustration of two interacting heptad repeats of a dimeric coiled-coil. Green circles represent hydrophobic amino acids. The red/blue circle highlights the position of charged amino acids and their electrostatic interactions. The remaining yellow circles indicate hydrophilic amino acids.

The **e** and **g** position contain oppositely charged amino acids, which have great influence on the pairing specificity of the helices. Most abundant at these positions are lysine and glutamic acid, respectively. The interhelical charge interaction acts between the **g** position of one heptad and the **e** position of the following repeat (Fig. 1-1). [9] The electrostatic interactions caused by the opposite charge of the amino acids stabilize the coil and determine the pairing. The charge pattern dictates the preference for homo- or heterotypic pairing as well as the orientation of the coil (parallel or antiparallel). [14] Exchanging an attractive **g**-**e** pair with repulsive amino acids leads to a destabilization of the coiled-coil. [15] However, Arndt and coworkers created a peptide library of Jun-Fos heterodimers, which shows data deviating from the PV hypothesis. [16] During their *in vivo* selection process, where variable pairs at the **e** and **g** positions were used, the optimal

coiled-coil contained two repulsive pairings. An even higher thermodynamic stability than a rationally designed coiled-coil could be achieved with this coiled-coil. This suggests, that other factors, which are not included in the PV hypothesis, play a role in the stability of coiled-coils.

The distribution of charged amino acids contributes additionally to the oligomerization state of coiled-coils. In coils with three or more helices, an increased amount of hydrophobic amino acids can be found at the **e** and **g** position. [12] The additional hydrophobic amino acids increase the width of the hydrophobic face, which is necessary for the extended interaction.

The remaining **b**, **c** and **f** position must be hydrophilic according to the PV hypothesis. These amino acids form the surface of the coiled-coil and are in direct contact with the environment. [9] As a consequence, as soon as a coiled-coil is exposed to an aqueous buffer the hydrophobic and hydrophilic amino acids arrange themselves the same way as during the folding of globular proteins.

The PV hypothesis states several requirements for the formation of coiled-coils. However, several exceptions and deviations exist from this hypothesis, making it only a rough guideline. It also only covers the basic interactions for dimeric left-handed coiled-coils and some of their variations.

1.2 Self-assembling peptide nanotubes

Self-assembling peptide nanotubes typically consist of small and simple peptide building blocks. These building blocks have the ability to assemble spontaneously into nano structures of higher order. Such peptides can be quite easily combined with other building blocks, such as lipids, sugars or nucleic acids, which gives them an advantage over unreactive carbon nanotubes. [17] The versatility of PNTs along with their chemical and functional diversity drew great interest in the field of nanotechnology. Up to today, several types of building blocks have been discovered to form PNTs or peptide fibers. The simplest types of blocks are dipeptides, like the Alzheimer's beta-amyloid diphenylalanine motif. [18] These peptides form highly stable, stiff multiwall nanotubes, which have a diameter of 80 - 300 nm. Another type of building block are surfactant-like peptides, consisting out of a hydrophilic head and a hydrophobic tail, which create nanotubes built-up from a bilayer of peptides. [19] Moreover, cyclic peptides, with alternating D- and L-amino acids, have been reported to form peptide nanotubes. [20]

Several working groups also employed α-helical coiled-coils to form peptide fibers or PNTs. [21, 22]

Burgess and coworkers *de novo* designed a toolkit of coiled-coils, based on already known sequence-to-structure relationships. [23] Their peptide library includes different oligomerization states, ranging from dimers and trimers up to a heptamer. Pentamers and above show accessible lumens of their α-helical barrel. All of their peptides contain 28 amino acids, which form four heptad repeats and therefore eight helical turns. By having a various amount of hydrophobic amino acids and different positions of the charged amino acids, different oligomerization states could be achieved. Charged residues at the C-terminus, which is either a lysine or a glutamic acid, and an oppositely charged side chain at the N-terminus, provide the necessary electrostatic interactions of the barrels to assemble into tubes (Fig. 1-2).

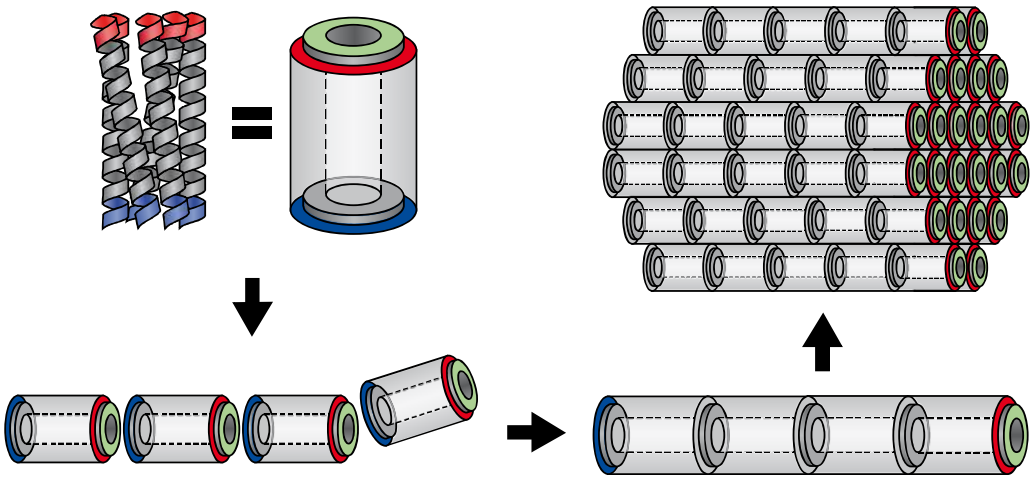

Figure 1-2 Schematic illustration of the proposed end-to-end assembly of the coiled-coil PNTs. Oppositely charged residues at the C- and N-termini are indicated with red and blue, respectively. Green highlights exposed patches of the hydrophobic core. [23]

Patches of the hydrophobic core and free carboxy and amino termini should further promote an end-to-end assembly of the formed α-helical barrels. With this design, kinetically stable fibers and tubes are obtained upon dissolution in aqueous buffer. The fibril formation can already be observed at low peptide concentrations (~40 µM) and yields fibers/tubes with a diameter of 15 to 65 nm. The thickened fibers can be explained by further fibril-fibril interactions, which are caused by the symmetrical lateral assembly of the building blocks. Thermal annealing of the fibrils leads to a further enhancement of this thickening.

In the course of this work a pentamer (CC-Pent-T) and a hexamer (CC-Hex-T) from the toolkit of Burgess *et al.* were used and further modified. [23]

1.3 Functionalization of peptide nanotubes

Peptide nanotubes have found use in a broad range of applications, such as biosensors, energy storage devices, tissue engineering or for drug delivery. [24, 25, 26, 27] However, often a combination of PNTs with specific binding motifs or other functional groups is necessary for these applications. To enhance their ability as drug delivery system, Sanchis *et al.* conjugated PNTs with polymers. This allowed them to tune their solubility, size and introduce further functionality. [28] Peptide nanotubes, functionalized with folic acid, enable the selective detection of human cervical cancer cells, which overexpress folate receptors. [29] MacCuspie and coworkers even combined PNTs with antibodies to create a method for high sensitive detection of viruses. Their developed fluorescent nanotubes aggregate around its target and form a network structure, allowing it to detect low number of viruses. [30]

However, most of these modifications are introduced after the peptides are assembled into nanotubes. Functionalizing the peptide building block prior to the self-assembling often results in a loss of its ability to assemble into higher ordered structures. For coiled-coils only a few possible sites to introduce modifications are conceivable. For the peptide back-bone an additional chemical functionalization will most likely result in a loss of the α-helical structure of the coil. Since the termini as well as the charged and hydrophobic side chains are essential criteria for the formation of the coiled coil and its further assembling into fibers, they are excluded as possible candidates as well.

This leaves only the side chains of the amino acids from the outer surface as possible modification sites. Regarding the supposed assembly of CC-Pent-T (Fig. 1-3), the **b** (Q) or **f** (X) position would be suitable. For CC-Hex-T, the **c** (A) or **f** (X) position are eligible. In the design of CC-Hex-T and CC-Pent-T combinations of lysine, glutamine and tryptophan were used for **f** only to favor helicity, to improve solubility or to provide a UV chromophore. A redesign of CC-Hex-T, where three amino acids of the **f** position were replaced with a lysine, resulted in single nanotubes with a diameter of around 3 - 4 nm. [22] This data indicates, that the **f** position has only a major influence on the lateral assembly of the fibers and not on the stacking of the α-helical barrels. Additionally, having a free amine group from the lysine makes it convenient to couple further amino acids on the

coil. One goal of this work was the functionalization of these two peptides by introducing a silaffin peptide motif at the **f** position.

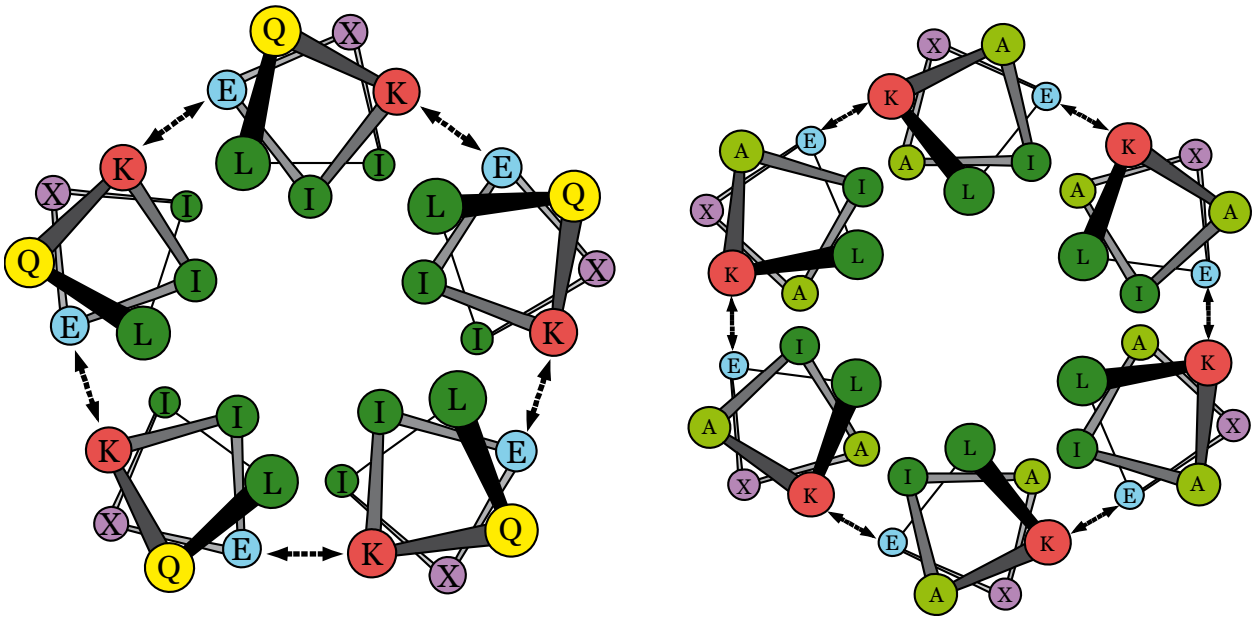

Figure 1-3 Proposed coiled-coil assembling of CC-Pent-T (left) and CC-Hex-T (right). Green circles represent hydrophobic amino acids, red/blue circles charged amino acids and yellow circles hydrophilic amino acids. Purple circles represent either lysine, glutamine or tryptophan. [23]

1.4 Diatoms and silaffin proteins

Diatoms are one of the largest and most important groups of organisms in the world since they have a huge ecological impact with their assimilation of carbon dioxide. Around 20 Gt of carbon dioxide are fixated annually by diatoms, which is about 20% of the worldwide assimilated CO_2 by photosynthesis, more than all of the rainforests combined. [31] Diatoms can be found nearly everywhere as long as there is sufficient water and light. They are an easily identifiable species, because of their exceptional cell structure. Their cell design is unusual, because of their silica associated cell wall. The shape of the cell wall varies for different species of diatoms, but they can be described as straight, closed cylinders. Their cross section can range from simple circles or ellipses to even more complex shapes (Fig. 1-4). Overall about 10,000 species of diatoms are listed, but over 200,000 species are estimated to exist. [32]

Figure 1-4 Scanning electron micrographs of different diatom species. [42]

During the vegetative reproduction of diatoms, the newly formed daughter cell as well as the original cell have to newly form half of their silica cell wall. [33] For this purpose, diatoms enrich silica intracellularly from their environment in the form of silicic acid. [34] Transmembrane proteins, called silicic acid transporter proteins (SITs), actively transport the silicic acid into the cell. [35] The synthesis of the new cell walls is later initiated in silica deposition vesicles (SDVs). [36] Kröger *et al.* discovered two main classes of biomolecules, which are responsible for the biomineralization process: Long chain polyamines (LCPAs) and silaffins. [37, 38] However, several organic molecules besides those two are essential for the correct formation of the cell walls.

1.5 Biomineralization with silaffins

Silaffin proteins were firstly discovered in the pennate diatom *Cylindrotheca fusiformis* during a cell wall extraction with ammonium fluoride. [38] The high affinity of the proteins to silica led to their naming as silaffins. The treatment of the extract with anhydrous HF led to the discovery of the three proteins named silaffin-2 (17 kDa), silaffin-1B (8 kDa) and silaffin-1A (4 kDa) (Fig. 1-5, A). The screening of a *C. fusiformis* genomic library with a cDNA of silaffin-1B led to the identification of sil1. The 795 base pair long open reading frame of sil1 encodes a polypeptide of 265 amino acids (sil1p) (Fig. 1-5, B). The first amino acids of its sequence (residues 1 - 19) represent a typical signal sequence, which is responsible for the translocation into the endoplasmatic reticulum. This part is followed by a sequence containing a high percentage of acidic amino acids (residues 20 – 107), with a still unknown function. The remaining sequence consists of seven nearly homologous units, with varying amounts of residues. These repeating units, which are

denoted with R1 to R7, contain high amounts of basic amino acids in the form of clustered lysine and asparagine. In between these clusters, mainly the amino acids serine and tyrosine are present.

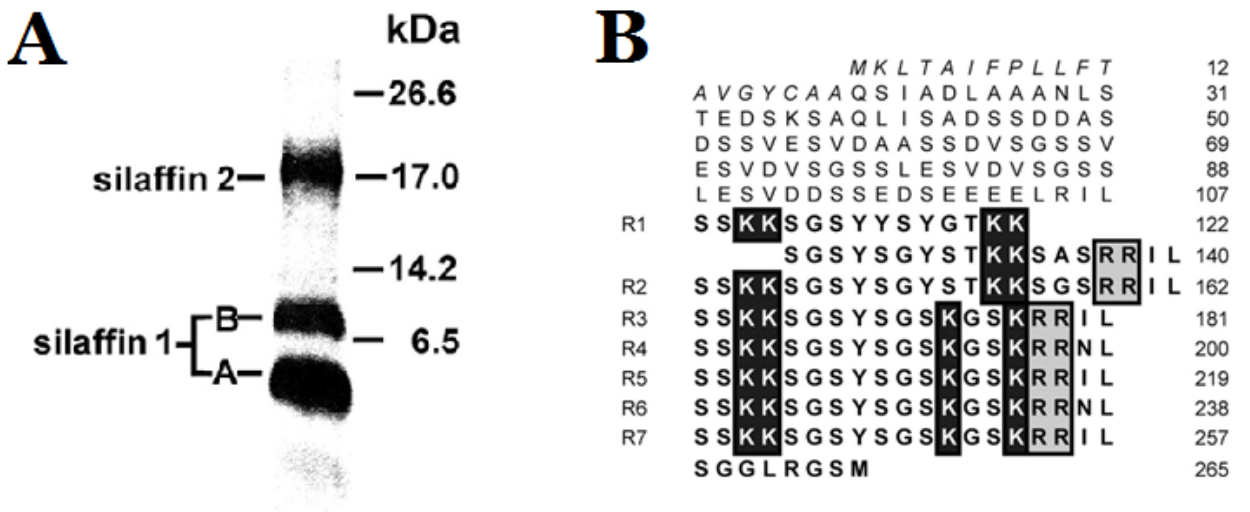

Figure 1-5 **A)** SDS-Page of HF treated ammonium fluoride extracts from *C. fusiformis*. **B)** Primary structure of the precursor protein sil1p. Repetitive elements are denoted with R1 – R7. Additionally, lysine and asparagine clusters are highlighted. [38]

The N-terminal part of silaffin-1B can be assigned to the amino acids 108 to 120 from the R1 unit. The first 11 amino acids of the repeats R2 to R7 match the N-terminus of silaffin-1A. Silaffin-1A can be further divided into silaffin-$1A_1$ (originating from R2) and silaffin-$1A_2$ (originating from R3 – R7). This indicates that silaffin-1A and -1B both originate from a proteolytic processing of sil1p. Later experiments by Kröger *et al.* revealed numerous additional posttranslational modifications. [39, 40] Silaffin-$1A_2$ contains two lysine residues, where the ε-amino group is linked to a linear polyamine consisting of 5 to 11 N-methylated propylamine units. These polyamine modifications have a strong resemblance with the LCPAs, which are also contained in the cell wall. The remaining two lysine residues are methylated to ε-N,N-dimethyllysine. Additionally, in Silaffin-$1A_1$ a lysine derivative, with a quaternary ammonium group, was discovered. It was the first peptide shown to contain ε-N,N,N-trimethyl-δ-hydroxylysine as a modification (Fig. 1-6). [40]

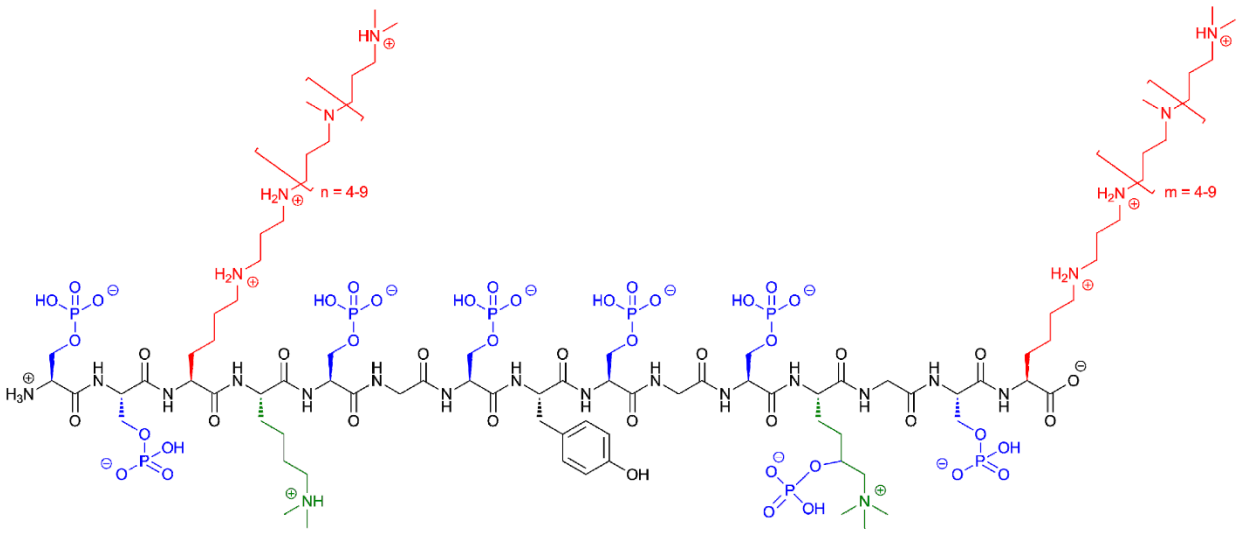

Figure 1-6 Full chemical structure of the native silaffin-1A$_1$ including its post-translational modifications at pH 5. [41]

Switching to milder extraction conditions with aqueous ammonium fluoride revealed additional modifications, which were cleaved during the extraction with HF. All seven serine hydroxyl groups are phosphorylated in the native form of silaffin-1A$_1$ (natSil-1A$_1$). [39] A phosphorylation was also found at the trimethylated lysine residues, which are hydroxylated and phosphorylated at their δ-position. Ionized groups can be found on eleven out of 15 residues, leading to an accumulation of positive as well as negative charges. ^{31}P-NMR spectroscopy indicated, that the zwitterionic state of natSil-1A causes a self-assembly via electrostatic interactions. Kröger *et al.* hypothesized, that the self-assembly is essential for the silica biomineralization, by providing a template for the polycondensation of the silicic acid.

Silaffins not only possess the ability to precipitate silica *in vivo* but also *in vitro*. Both silaffin-1A$_1$ and silaffin-1A$_2$ precipitate silica nanospheres, when silicic acid is added at a pH < 7. The native form silaffin-1A$_1$ can precipitate silica immediately from a solution of silicic acid. [40] However, silaffin-1A$_1$, lacking the phosphorylation at the serine residues, is unable to precipitate any form of silica under the same conditions. Adding phosphate anions to the solution leads to the restoration of the precipitation ability. At low concentrations of phosphate, the amount of precipitated silica is decreased, indicating that phosphate ions are indeed a limiting factor. If silicic acid and phosphate anions are available in excess, the amount of precipitate is directly proportional to the amount of silaffin. [39] The peptides themselves coprecipitate with the silica during the reaction. The diameter of the formed silica particles ranges between 500 and 700 nm. [40]

Not only the silaffins are capable of biomineralization, but also LCPAs have shown the ability to precipitate silica. [40] However, the addition of phosphate ions is also required. Synthetic derivatives from the repetitive units of sil1p also possess this property. The R5 peptide, which is the 5th repetitive unit from sil1p with an additional N-terminal cysteine, precipitates analogous spherical silica nanoparticles (Fig. 1-7 A). Yet, the C-terminal RRIL sequence, which is not present in the silaffins, is required for an effective precipitation. The significance of the RRIL sequence is still not fully understood but it could be shown that its position has a major influence on the shape of the particles (Fig. 1-7, B). [41]

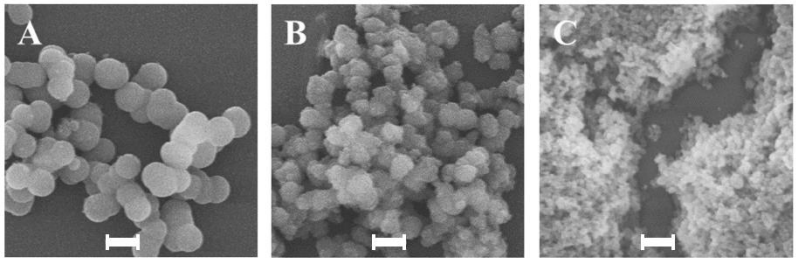

Figure 1-7 Scanning electron micrographs of silica particles from different peptides. **A)** R5 peptide. **B)** R5 peptide with RRIL moved to the N-terminus. **C)** truncated R5 peptide only consisting of KRRIL. Scale bars: 1 µm. [41]

It could also be demonstrated that the lysine residues are active elements in the mechanism of silica precipitation, since a mutation to alanine in the R5 peptide resulted in a loss of the ability to precipitate silica. A truncated version of the R5 peptide, which consists only of a lysine and the C-terminal RRIL, is the shortest peptide known to be able to precipitate silica. However, the precipitate has not a defined spherical shape, which could be due to an inhibited self-assembling of the peptide. [41] The short KRRIL sequence is the second building block, used in this work in order to obtain silica nanotubes.

1.6 Silica nanoparticles in biotechnology

The interest in mesoporous silica nanoparticles (MSNs) increased drastically when it could be demonstrated that the particles can be loaded with anti-inflammatory drugs. Vallet-Regi and coworkers showed that MSNs can be loaded with the drug ibuprofen, which was sustainably released afterwards. [43] MSNs are readily internalized by eukaryotic cells, which makes them suitable as novel form of drug delivery system. [44]
The loading of mesoporous silica nanoparticles can be achieved in two different ways. In a first approach, the cargo molecule is covalently linked to the silica, which requires the

functionalization of the silica surface. [45] A more common used approach is the immersion loading method, which involves the soaking of the particles in a solution of the cargo molecules. [46] However, the loading efficiency of this process is dependent on several factors, like the pore size or the surface functionalization of the silica. [47] By tuning the pore size, large biomolecules, such as peptides or even proteins, can be loaded into the particles. [48] By modifying functionalized nanoparticles with targeting moieties, such as folic acid or antibodies, a specific targeting of cancer cells can be achieved. [49, 50] A targeted therapy with a controlled drug release implicates lower drug doses and can minimize the systemic toxicity of the drug. In summary, MSNs are interesting as a new form of drug delivery system by providing important properties such as tunable loading and release characteristics, target specificity and alterable morphology. Combining mesoporous silica with magnetite or other materials can further enhance these attributes or add additional properties. [51]

Furthermore, the surface properties and the small particle size allows MSNs to be used in biosensing applications. The high surface area and the abundance of ordered pores allows a high concentration of accessible receptor molecules. Additionally, an increased chance to detect large molecules and a faster diffusion rate to the receptor location results in an efficient performance of the sensors. Studies demonstrated, that mesoporous silica loaded with glucose oxidase and horseradish peroxidase can be used as sensors for glucose. [52] Likewise, silica modified electrodes with immobilized myoglobin and hemoglobin are utilized as sensors for H_2O_2 and NO_2^-. [53]

The major disadvantage of mesoporous silica particles is often a complicated synthesis, which requires harsh reaction conditions. It is still impossible to obtain silica in highly ordered structures, which can only be found in nature. For this reason, biogenic or biomimetically formed silica draws more and more attention in science. [41]

2 Objective

Mesoporous silica nanoparticles have found great use in a variety of biotechnological applications, including drug delivery or as biosensors. However, a major disadvantage of MSNs lies in their complicated synthesis, which requires among other things harsh reaction conditions. For this purpose, it would be advantageous to have biomimetically formed silica particles specifically tailored for different applications.

The main goal of this work is the combination of two simple peptide building blocks to obtain tailored silica nanotubes. The first building block was adapted from the toolkit of Burgess *et al.*. Their designed peptides are derived from coiled-coil sequences with known sequence-structure relationships, which assemble into α-helical barrels. Their toolkit includes peptides with different oligomerization states and peptide nanotubes (PNTs) with different dimensions and accessible lumens. Furthermore, their short sequence consisting of heptad repeats allows a simple synthesis and the introduction of additional modifications. Moreover, the stability of the coiled-coil motif makes their peptides convenient templates for the formation of silica nanotubes.

The second building block has to enable the formation of silica around the template peptide nanotube. Silaffin proteins, which are derived from diatoms, possess the ability to precipitate silica from silicic acid. Synthetic derivatives of these silaffins, such as the R5 peptide, have also been reported to successfully precipitate silica *in vitro*. However, mainly spherical particles have been observed, which is probably caused by the aggregation of the silaffins. The KRRIL motif is a short sequence found in silaffins, which is still able to precipitate silica from silicic acid. However, the formed silica lacks its defined morphology, which is probably the result of a disturbed assembling of the peptides.

To target the goal of silica nanotubes, combinations of these two building blocks are tested. Attaching the KRRIL motif on the surface exposed side chains of the coiled-coil peptides can be achieved by coupling to the ε-amino group of a lysine in the **f** position of a heptad repeat. This should still allow a proper interaction of the coiled-coils to assemble into α-helical barrels and further into PNTs, with multiple KRRIL moieties on its surface (Fig. 2-1). CD spectrometry, scanning electron microscopy and dye intercalation assays can be performed to confirm the secondary structure and higher assembly of the peptides. The addition of silicic acid *in vitro* should lead to a precipitation of silica by the KRRIL motif giving silica encapsulated PNTs. Removing the organic material from the obtained

silica nano tubes can be achieved by calcination afterwards. The tunable characteristics of the template peptide and different concentrations of silica could further allow different sizes and thicknesses of the silica tubes. This should enable us to adjust the silica tubes depending on the area of application.

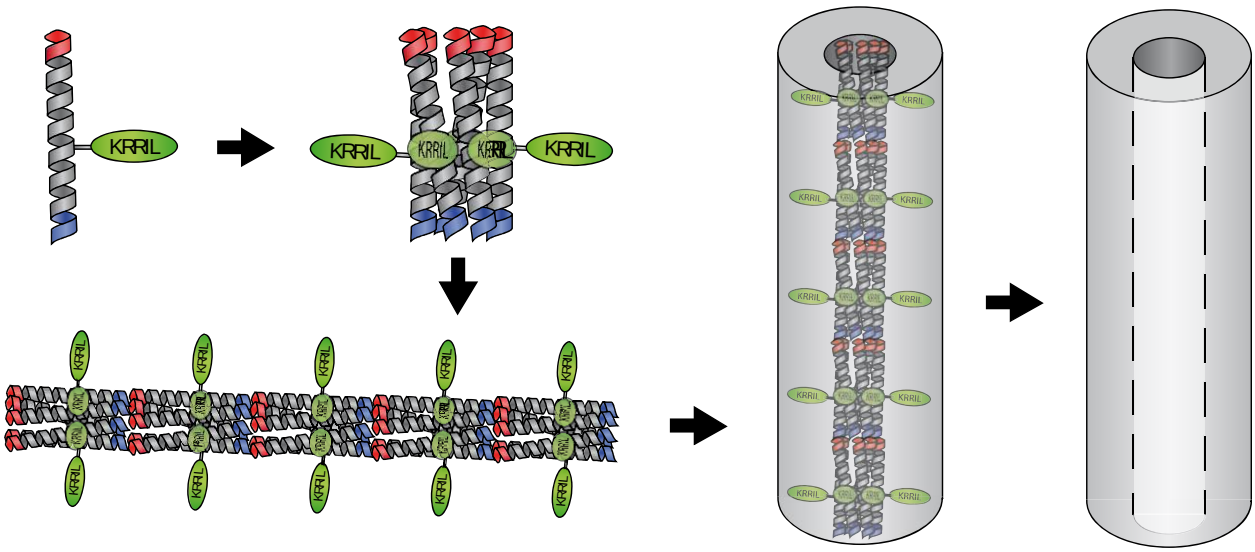

Figure 2-1 Strategy overview to obtain silica nano tubes. A combination of the KRRIL moiety and a coiled-coil peptide lead to the formation of PNTs with the KRRIL sequence exposed on its surface. *In vitro* silica precipitation leads to coating of the PNT with silica. Removal of the peptide is achieved by calcination.

3 Materials and Methods

3.1 Chemicals

The following chemicals and solvents were obtained from different commercial sources and used without further purification: Fluorenylmethoxycarbonyl (Fmoc) protected amino acids, 2-(1H-benzotriazol-1-yl)-1,1,3,3-tetramethyluronium hexafluorophosphate (HBTU), guanidine hydrochloride and ethanol (Merck, Germany); acetonitrile (ACN), ninhydrine, *N,N*-diisopropylethylamine (DIEA), *N,N′*-diisopropylcarbodiimide (DIC), 1,6-diphenyl-1,3,5-hexatrien (DPH), oxyma pure, triisopropylsilane (TIPS), phenol, potassium cyanide (KCN), pyridine and dulbecco's phosphate buffered saline (PBS) (Sigma-Aldrich, US); *tert*-butyloxycarbonyl (Boc) protected amino acids (ORPEGEN Peptide Chemicals, Germany); Fmoc-Glu(OtBu)-TentaGel™-resin and Fmoc-Lys(Boc)-TentaGel™-resin (Rapp polymers, Germany); Fmoc-Lys(Boc)-Wang-resin (Iris Biotech, Germany); *N,N*-dimethylformamide (DMF), trifluoroacetic acid (TFA) (Carl Roth, Germany); dichloromethane (DCM) (Biosolve, Netherlands); aceton (VWR, Austria); diethylether (neoLab, Germany).

ddH2O was generated using a Milli-Q® Reference (Merck Millipore, Germany) water purification system.

KRRIL peptide, linked to Wang-resin and missing the N-terminal lysine, was synthesized by solid phase peptide synthesis and received from Patrick Capel.

Cy5-carboxylic acid was obtained from Meder Kamalov and was used without further purification.

3.2 Peptide synthesis and purification

3.2.1 HPLC and mass spectrometry

Peptide purification:

For purification of peptides a Waters Auto-Purification HPLC/MS system (Waters GmbH, Germany) was used (3100 Mass Detector, 2545 Binary Gradient Module, 2767 Sample Manager and 2489 UV/Vis Detector). UV/Vis traces were recorded at 214 and 280 nm. As solid phase, either a Kromasil 300—10-C4 column (250 x 20 mm, 10 µm particle size) or semi-preparative Kromasil 300-10-C4 column (250 x 10 mm, 10 µm particle size) were used. Mass spectra were obtained by electrospray ionization mass spectrometry (ESI-MS), operating in positive ion mode. As solvents buffer A (ddH_2O +

0.05% TFA) and buffer B (ACN + 0.05% TFA) were used. UV/Vis traces were recorded at 214 and 280 nm.

Analytical runs:

Analytical RP-HPLC runs were performed on a Dionex Ultimate 3000 (Thermo Fisher Scientific, US). As solid phase, either a 300—5-C4 column (150 x 4.6 mm, 5 µm particle size) or 300-5-C4 column (250 x 4.6 mm, 5 µm particle size) were used. Mass spectra were obtained by electrospray ionization mass spectrometry (ESI-MS), operating in positive ion mode. As solvents buffer A (ddH_2O + 0.1% TFA) and buffer B (ACN + 0.1% TFA) were used. UV/Vis traces were recorded at 214 and 280 nm.

3.2.2 General protocol for solid phase peptide synthesis (SPPS)

All syntheses were performed using fluorenylmethoxycarbonyl chemistry on either preloaded Wang-polysterene or TentaGel™ resins. The Fmoc-protected preloaded resin was weighted into a syringe, depending on the scale used and the loading value of the resin, and swollen in DMF for at least 2 h under stirring. Fmoc-deprotection of the amino acids was achieved with a solution of 20% piperidin in DMF in two cycles of 3 min and 7 min with DMF washing steps in between. Afterwards, the activated amino acids were added and coupled for 40 min. Double couplings were only performed in the case of Arginine. For double couplings, the first coupling solution was removed and a second activated amino acid mixture was added and incubated again for 40 min. Kaiser tests were occasionally done before and after the coupling or deprotection to ensure the proper coupling of the amino acid or the removal of the Fmoc group. Furthermore, test cleavages were performed to ensure the quality of the synthesis.

Activation of the amino acids was achieved by mixing 2.5 eq. amino acid with 2.38 eq. of HBTU (0.5 M in DMF) and stirring the solution for 1 min or until the peptide was dissolved. 5 eq. of DIEA were added afterwards and mixed again for 3 min. The activated amino acid was subsequently added to the solid support.

3.2.3 Automated Liberty Blue synthesis

Automated SPPS syntheses were performed using a CEM Liberty Blue Microwave Peptide Synthesizer (CEM GmbH, Germany). All syntheses were carried out using Fmoc-

chemistry with the integrated standard conditions and in a 0.1 mmol scale. Analogue to the manual syntheses, Fmoc-aa preloaded resins were used in all cases. Oxyma pure and DIC were used for the activation of the amino acids.

3.2.4 Peptide cleavage from solid support

After the peptidyl resin was washed several times with DCM, the resin was dried under vacuum. Afterwards, a cleavage solution of 5% (v/v) triisopropylsilane, 2.5% (v/v) ddH_2O and 92.5% (v/v) TFA was applied to the peptidyl resin. The used volume was around 5 times than the volume of the dried resin. For the Cy5 modified peptides, a cleavage cocktail consisting of 5% (v/v) thioanisole, 5% (v/v) ddH_2O, 2.5% (v/v) 1,2-ethanedithiol (EDT), 5% (v/v) phenol and 82.5% (v/v) TFA was used. The peptidyl resin was stirred together with the cleavage cocktail for 4 h. For test cleavages, the cleavage cocktail was applied for 2 h only. Afterwards, the peptide was precipitated with 5 vol. eq. cold diethylether (Et_2O). The solvent was removed after centrifugation and the peptide resuspended in cold Et_2O. The washing step with Et_2O was repeated for two more times. The obtained peptide pellet was dried with nitrogen gas, dissolved in 50:50 buffer A:B and lyophilized to complete dryness.

3.2.5 Removal of 4-methyltrityl (Mtt) from amino acid side chains

Peptidyl resin was washed several times with DCM and swollen/rebuffered in DCM for at least 2 h. For the removal of Mtt, a solution of 98% DCM, 1% TIS and 1% TFA was prepared. 5 mL of the cleaving solution were added to the peptide and agitated for 2 min. During the deprotection, a yellow coloring of the solution appeared. The resin was washed with DCM until the yellow color disappeared. The procedure was repeated, until the yellow coloring vanished, when the deprotecting solution was added. For 0.05 mmol of 4-methyltrityl, around 170 mL of DCM/TIS/TFA solution had to be used. The peptidyl resin was washed several times with DMF afterwards and rebuffered in DMF for 2 h, before it was further used.

3.2.6 Kaiser Tests

Kaiser tests were performed to confirm or confute the presence of free amino groups during peptide synthesis. Few peptidyl resin beads were washed several times with DCM

and dried under vacuum. 30 µL phenol solution (80% phenol in ethanol), 30 µL KCN solution (0.02 M KCN in Pyridine) and 30 µL ninhydrin solution (6% ninhydrin in Ethanol) were added. The reaction mixture was heated up to 90°C for 3 – 5 min. The color of the solution was used to assess the presence of free amino groups. A blue to purple color indicates the formation of Ruhemann's purple, which is only possible when primary amines are present. This positive result either indicates a proper deprotection of an amino acid or only partial coupling of an amino acid during synthesis. A yellow color after heating of the mixture is mainly caused by an iminium salt, which is formed by the reaction of ninhydrin with secondary amines. This negative result either indicates an improper deprotection of an amino acid or a successful coupling of an amino acid during synthesis.

3.3 Determination of peptide concentrations

To determine peptide concentrations, a NanoDrop 2000c UV-Vis Spectrophotometer (Thermo Scientific, US) was used. All measurements were done in PBS buffer and using the calculated molar extinction coefficients of the peptides. Pure PBS buffer was used to create a reference baseline.

Peptide	**Calculated molar extinction coefficient (M^{-1} cm^{-1})**
CC-Pent-T	5500
CC-Pent-Mod-1	5500
CC-Pent-Mod-2	5500
CC-Hex-T	5500
CC-Hex-Mod-1	5500

3.4 Scanning electron microscopy

Dissolved and incubated peptide samples were applied on a Thermanox® plastic coverslip (Thermo Scientific, US) and incubated for 5 min at room temperature. The liquid was wicked off with filter paper afterwards. The samples were washed twice with water, by adding 5 µL of water on the coverslip and removing it with filter paper after 1 min. All samples were air dried at room temperature subsequently.

Samples from precipitation experiments were suspended in water, applied to a Thermanox® plastic coverslip and air dried at room temperature.
The coverslips were mounted on alumic sample holders and sputter coated with a 5 nm layer of gold. Sputtering was performed in high vacuum, using a Leica SCD050 (Leica Microsystems, Germany). SEM micrographs at different magnifications were obtained using a Zeiss Supra 55 VP (Carl Zeiss, Germany) scanning electron microscope (SEM) operating at 5 kV.

3.5 Circular Dichroism (CD)

All far UV-CD spectra were obtained, using a Chirascan Plus spectrometer (Applied Photophysics, UK). Measurements were performed at room temperature in a 1 mm quartz cuvette, at 1 nm resolution and with 1 s acquisition time. The wavelength range was between 200 and 260 nm. For all proteins ten spectra were recorded and averaged. All proteins were dissolved in PBS at a concentration of 0.1 mM.
To obtain the composition of the secondary structures, CDNN software was used. Peak maxima at 193 nm and peak minima at 208 and 222 nm were used to calculate the percentage of α-helices. For anti-parallel β-sheets, maxima at 195 nm and peak minima at 218 nm were considered. Random coils were identified, by a negative band around 195 nm and a low ellipticity above 210 nm.
The neuronal network of the CDNN software was trained, using several spectra from the database. Obtained averaged spectra were deconvoluted to calculate the percentage of α-helices, antiparallel and parallel β-sheets, β-turns and random coils.

3.6 1,6 diphenyl 1,3,5-hexatrien (DPH) intercalationassay [23]

All peptides were dissolved in PBS buffer at a concentration of 0.1 mM and incubated for at least 72 h before the assay. The assay was carried out in a 96 well-plate at room temperature. A dilution series with the following concentrations was prepared by diluting with PBS: 100 µM, 50 µM, 25 µM, 12.5 µM, 6.3 µM, 3.1 µM, 1.6 µM, 0.8 µM, 0.4 µM, 0.2 µM, 0.1 µM and 0 µM. DPH dissolved in acetone was added to the peptides to a final concentration of 1 µM. The peptide and DPH mixtures were left at room temperature to equilibrate for 3 h. Fluorescence spectra were acquired using a BioTek Synergy Mx Microplate Reader (BioTek, US). The spectra were recorded between 380 and 600 nm

with an excitation wave length of λ_{ex} = 350 nm. The obtained fluorescence at 455 nm was normalized to the highest value to facilitate a direct comparison.

3.7 Time resolved assay

CC-Pent-T and CC-Hex-T were dissolved in PBS buffer at a concentration of 0.1 mM and incubated for at least 72 h before the assay. Additionally, a freshly dissolved sample of both peptides (0.1 mM) was prepared prior to the assay. The assay was carried out in a 96 well-plate at room temperature. A dilution series with the following concentrations was prepared by diluting with PBS: 25 µM, 12.5 µM, 6.3 µM, 3.1 µM, 1.6 µM, 0.8 µM, 0.4 µM, 0.2 µM, 0.1 µM and 0 µM. All concentrations were measured in triplicates. DPH dissolved in acetone was added to the peptides to a final concentration of 1 µM. Fluorescence was recorded at 455 nm using a BioTek Synergy Mx Microplate Reader (BioTek, US) with an excitation wave length of λ_{ex} = 350 nm. Measurements were done every 10 minutes for a period of 18 h at room temperature.

3.8 Size analysis of particles and nano tubes

Size analysis of the particles and nano tubes was done with ImageJ. To obtain a statistical distribution of the sample, a representative number of particles and PNTS was analyzed. Diameters and lengths were directly obtained from the corresponding electron micrographs.

3.9 Silica precipitation *in vitro*

Peptides, which were used for the precipitation, were dissolved in PBS buffer at a concentration of 0.1 mM at pH 7.4. The dissolved peptides were incubated in the buffer at room temperature for at least 24 h before the precipitation. Silicic acid was obtained, by hydrolysis of 37 µL (250 µmol) tetramethoxysilane (TMOS) in 1 mL of 1 mM aqueous HCl for 4 min. The precipitation reaction was initiated by the addition of silicic acid to the peptide solution, resulting in a final concentration of silicic acid of 25 mM. All samples were shaken and incubated at room temperature for 30 min. The precipitate was removed from the supernatant by centrifugation and washed twice with water.

3.10 Energy-dispersive X-ray spectroscopy (EDX)

Dissolved and incubated peptide samples were directly applied to the alumic sample holder and air dried at room temperature. This process was repeated several times to obtain sufficient peptide for the analysis. The peptides were washed twice with water as described in 3.4.

Samples from precipitation experiments were suspended in water, applied directly to the alumic sample holder and air dried at room temperature. This process was repeated several times.

Energy-dispersive X-ray analysis was performed on a Zeiss Supra 55 VP, operating at 20 kV. An X-ray detector from Oxford Instruments (UK) was used to obtain the spectra.

3.11 Thermal annealing of peptides

Thermal annealing of the peptides was attempted using a MJ Mini Thermal Cycler (Bio-Rad Laboratories, US). Peptide samples were dissolved in PBS buffer at a concentration of 0.1 mM and incubated at room temperature for at least 72 h. CC-Pent-T and CC-Pent-Mod-1 were mixed together prior to the annealing (final concentrations: CC-Pent-T = 75 µM; CC-Pent-Mod-1 = 25 µM). Samples were heated from 20 to 95°C over 180 min, followed by a cooling to 25°C in 20 min. Samples were either incubated again for 24 h at room temperature or directly used for an *in vitro* silica precipitation.

3.12 Calcination of silica nano tubes

For the attempted calcination of the silica nanotubes a Galen III melting point meter (Leica Camera, Germany) was used. 500 µL of nanotubes, suspended in ddH_2O, were applied on a glass slide and heated to 50°C in 15 min. After 30 min at 50°C, the sample was heated to 240°C in 1.5 h. The sample was incubated at that temperature for an additional 30 min. Afterwards, the silica particles were resuspended in ddH_2O, applied on a sample slide for SEM and dried at room temperature. Analysis of the sample was done analogous to the description in 3.4.

3.13 Fluorescence microscopy

An ELYRA PS.1 and LSM 710 Configuration 1 (Carl Zeiss, Germany) were used to obtain fluorescence images of the peptide (λ_{ex} = 620 nm, λ_{em} = 670 nm). To prepare CC-Pent-

Cy5 for the microscopy, the peptide was dissolved in PBS at a concentration of 0.1 mM and incubated at room temperature for 72 h. The incubated peptide was diluted with PBS afterwards to final concentration of 10 µM. The sample was placed between two microscope glass slides, which were fixated subsequently. An oil immersion objective was used for the sample magnification.

4 Results and Discussion

4.1 Peptide synthesis and purification

To observe the effect of an introduced modification on the PNTs, eight different peptides were synthesized. First of all, CC-Pent-T and CC-Hex-T, which are based on the studies of Burgess *et al.*, are used as references for unmodified PNTs. The short KRRIL sequence was synthesized to have a comparison of its ability to precipitate silica independently, and attached to another peptide. Three different modified forms of CC-Pent-T and one modified CC-Hex-T were designed in the progress of this work. The first set of peptides contain one introduced KRRIL sequence, coupled on the ε-amino group of the available lysine at the **f** position (CC-Pent-Mod-1 and CC-Hex-Mod-1). For the pentamer, an additional functionalized version was designed, containing two KRRIL sequences. For this purpose, a glutamic acid on the **f** position was replaced with a lysine to have a second ε-amino group (CC-Pent-Mod-2). To further investigate the assembly of the nanotubes, a version of the pentamer, functionalized with Cy5, was synthesized (CC-Pent-Cy5). Having a fluorescent group at the location of the KRRIL sequence could provide the possibility to gain insight on the assembly by fluorescence microscopy.

4.1.1Synthesis of CC-Pent-T

CC-Pent-T was synthesized manually on a 0.2 mmol scale, using the standard Fmoc-SPPS protocol. Preloaded Fmoc-Lys(Boc)-TentaGel™-resin (0.20 mmol/g loading) was used as solid support. The quality of the synthesis was monitored by test cleavages and Kaiser tests. After the synthesis, cleaving from the support was achieved, using the standard cleavage procedure. The peptide was purified by RP-HPLC (Waters AutoPurification HPLC/MS System, preparative C4 column, 20 mL/min flow rate, 25% to 65% buffer B (ACN + 0.08% TFA) in buffer A (ddH_2O + 0.08% TFA) in 40 min). Analytical RP-HPLC runs were performed on a Dionex Ultimate 3000 (analytical C4 column, 0.3 mL/min flow rate, 35% to 95% buffer B in buffer A in 30 min). The peptide was obtained in high purity and yielded 26.2 mg (15%).

Sequence: H- IEQI LQKIEKI LQKIEWI LQKIEQI LQK -OH

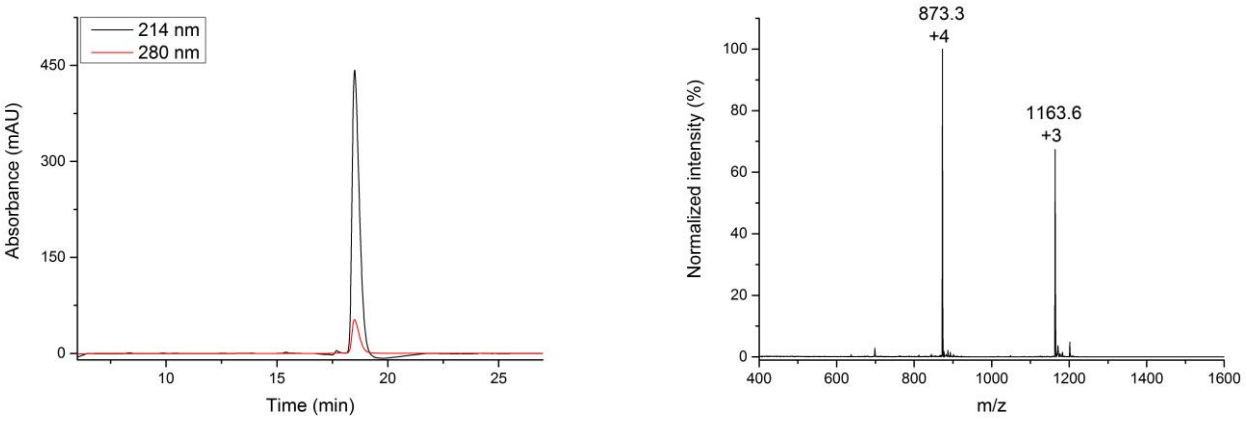

Figure 4-1 **Left)** Analytical UV chromatogram of CC-Pent-T after purification by RP-HPLC. **Right)** ESI-MS of purified CC-Pent-T. Calculated mass for $C_{163}H_{280}N_{40}O_{43}^{+}$: 3489.3 $[M+H]^{+}$. Observed masses: 1163.6 $[M+3H]^{3+}$, 873.3 $[M+4H]^{4+}$.

4.1.2 Synthesis of CC-Pent-Mod-1

The linear part of CC-Pent-Mod-1 was synthesized automatically on a 0.1 mmol scale, using Fmoc-SPPS on a Liberty Blue microwave peptide synthesizer. The N-terminal isoleucine was coupled with a Boc protection group instead of Fmoc. Fmoc-Lys(Mtt)-OH was used for the lysine at the **f** position to enable selective coupling on the ε-amino group. Preloaded Fmoc-Lys(Boc)-TentaGel™-resin (0.20 mmol/g loading) was used as solid support. The resin was split in half and selective removal of the Mtt group was performed. The remaining KRILL sequence was coupled manually, using the standard Fmoc-SPPS protocol. The quality of the synthesis was monitored by test cleavages and Kaiser tests. After the synthesis, cleaving from the support was achieved, using the standard cleavage procedure. The peptide was purified by RP-HPLC (Waters AutoPurification HPLC/MS System, preparative C4 column, 20 mL/min flow rate, 25% to 65% buffer B in buffer A in 40 min). Analytical RP-HPLC runs were performed on a Dionex Ultimate 3000 (analytical C4 column, 1.0 mL/min flow rate, 35% to 95% buffer B in buffer A in 30 min). The peptide was obtained in high purity and yielded 16.6 mg (8%).

Sequence: H- IEQI LQKIEKI LQKIEWI LQKIEQI LQK -OH
KRRIL ┘

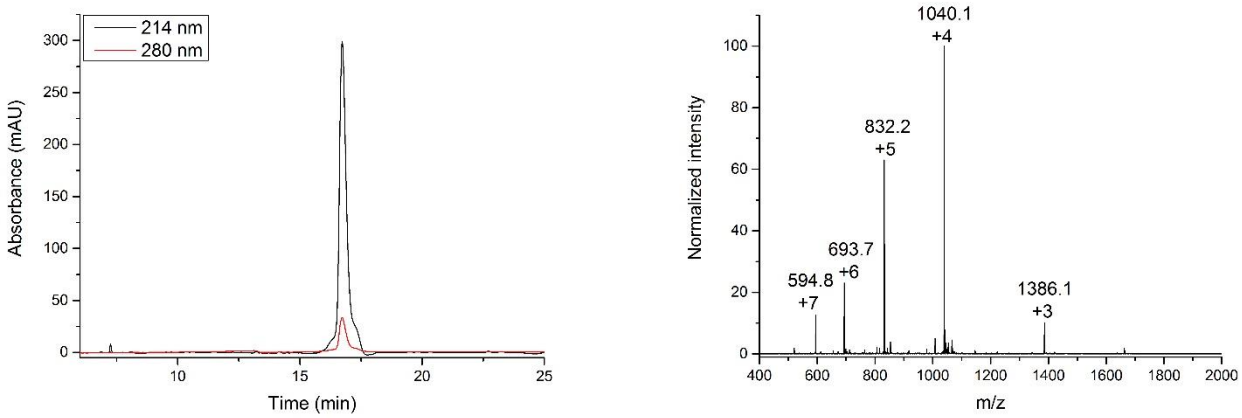

Figure 4-2 Left) Analytical UV chromatogram of CC-Pent-Mod-1 after purification by RP-HPLC. **Right)** ESI-MS of purified CC-Pent-Mod-1. Calculated mass for $C_{193}H_{338}N_{52}O_{48}^{+}$: 4156.1 $[M+H]^{+}$. Observed masses: 1386.1 $[M+3H]^{3+}$, 1040.1 $[M+4H]^{4+}$, 832.2 $[M+5H]^{5+}$, 693.7 $[M+6H]^{6+}$, 594.8 $[M+7H]^{7+}$.

4.1.3 Synthesis of CC-Pent-Mod-2

The linear part of CC-Pent-Mod-2 was synthesized automatically on a 0.1 mmol scale, using Fmoc-SPPS on a Liberty Blue microwave peptide synthesizer. The N-terminal isoleucine was coupled with a Boc protection group instead of Fmoc. Fmoc-Lys(Mtt)-OH was used for the lysines at the **f** positions to enable selective coupling on the ε-amino group. Preloaded Fmoc-Lys(Boc)-TentaGel™-resin (0.20 mmol/g loading) was used as solid support. The resin was split in half and selective removal of the Mtt group was performed. The remaining KRILL sequences were coupled manually, using the standard Fmoc-SPPS protocol. The quality of the synthesis was monitored by test cleavages and Kaiser tests. After the synthesis, cleaving from the support was achieved, using the standard cleavage procedure. The peptide was purified by RP-HPLC (Waters AutoPurification HPLC/MS System, preparative C4 column, 20 mL/min flow rate, 25% to 65% buffer B in buffer A in 40 min). Analytical RP-HPLC runs were performed on a Dionex Ultimate 3000 (analytical C4 column, 1.0 mL/min flow rate, 35% to 95% buffer B in buffer A in 30 min). The peptide synthesis yielded 13.3 mg (11%) of CC-Pent-Mod-2.

Sequence: H- IEQI LQKIEKI LQKIEWI LQKIEKI LQK -OH
KRRIL KRRIL

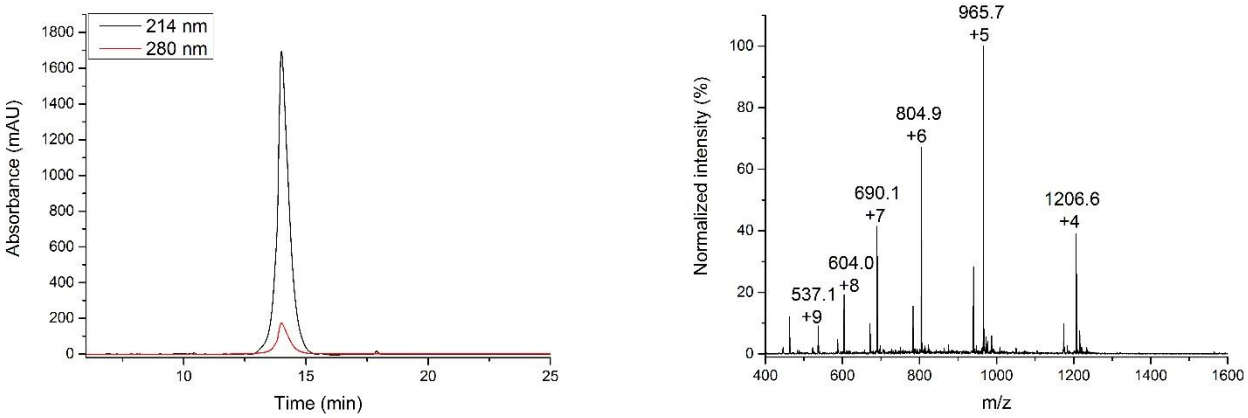

Figure 4-3 Left) Analytical UV chromatogram of CC-Pent-Mod-2 after purification by RP-HPLC. **Right)** ESI-MS of purified CC-Pent-Mod-2. Calculated mass for $C_{223}H_{396}N_{64}O_{53}^{+}$: 4823.0 $[M+H]^{+}$. Observed masses: 1206.6 $[M+4H]^{4+}$, 965.7 $[M+5H]^{5+}$, 804.9 $[M+6H]^{6+}$, 690.1 $[M+7H]^{7+}$, 604.0 $[M+8H]^{8+}$, 537.1 $[M+9H]^{9+}$

An impurity, with a mass of 4693.9 Da, can be observed in the chromatogram of the ESI-MS. Most likely, this impurity causes the broadening of the peak in the chromatogram. Due to the similar retention time as CC-Pent-Mod-2, a separation of both peptides was not possible. The mass difference of -147 Da is very likely caused by a missing glutamic acid. Since a high percentage of the obtained product consisted of the desired peptide and the effect of the missing charged amino acid is unknown, the obtained peptide was used for all further experiments.

4.1.4 Synthesis of CC-Pent-Cy5

The linear part of CC-Pent-Mod-Cy5 was synthesized automatically on a 0.1 mmol scale using Fmoc-SPPS on a Liberty Blue microwave peptide synthesizer. The N-terminal isoleucine was coupled with a Boc protection group instead of Fmoc. Fmoc-Lys(Mtt)-OH was used for the lysine at the **f** position to enable selective coupling on the ε-amino group. Preloaded Fmoc-Lys(Boc)-TentaGel™-resin (0.20 mmol/g loading) was used as solid support. The resin was dried and selective removal of the Mtt group was performed. Coupling of Cy5 was performed, using three different activators in a 0.005 mmol scale (Tab. 4-1).

Table 4 – 1 Used coupling conditions for the attachment of Cy5.

Coupling 1	Coupling 2	Coupling 3
1 eq. CC-Pent-T	1 eq. CC-Pent-T	1 eq. CC-Pent-T
3 eq. Cy5	3 eq. Cy5	3 eq. Cy5
2.38 eq. HBTU	2.38 eq. HATU	3 eq. Oxyma pure
5 eq. DIEA	5 eq. DIEA	3 eq. DIC

The quality of the synthesis was monitored by test cleavages and Kaiser tests. After the synthesis, cleaving from the support was achieved, using the standard cleavage procedure. The peptide was purified by RP-HPLC (Waters AutoPurification HPLC/MS System, semi-preparative C4 column, 10 mL/min flow rate, 25% to 65% buffer B in 40 min). Analytical RP-HPLC runs were performed on a Dionex Ultimate 3000 (analytical C4 column, 1.0 mL/min flow rate, 35% to 95% buffer B in 30 min).

Sequence: H- IEQI LQKIEKI LQKIEWI LQKIEQI LQK -OH

Cy5

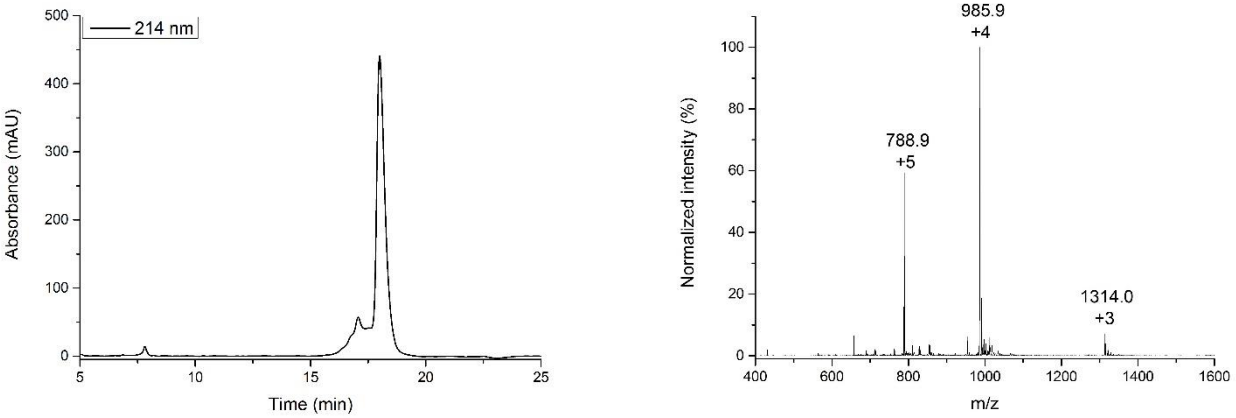

Figure 4-4 **Left:** Analytical UV chromatogram of CC-Pent-Cy5 coupled with HATU after purification by RP-HPLC. **Right:** ESI-MS of purified CC-Pent-Cy5. Calculated mass for $C_{194}H_{315}N_{42}O_{44}^{+}$: 3939.8 $[M+H]^{+}$. Observed masses: 1314.0 $[M+3H]^{3+}$, 985.9 $[M+4H]^{4+}$, 788.9 $[M+5H]^{5+}$.

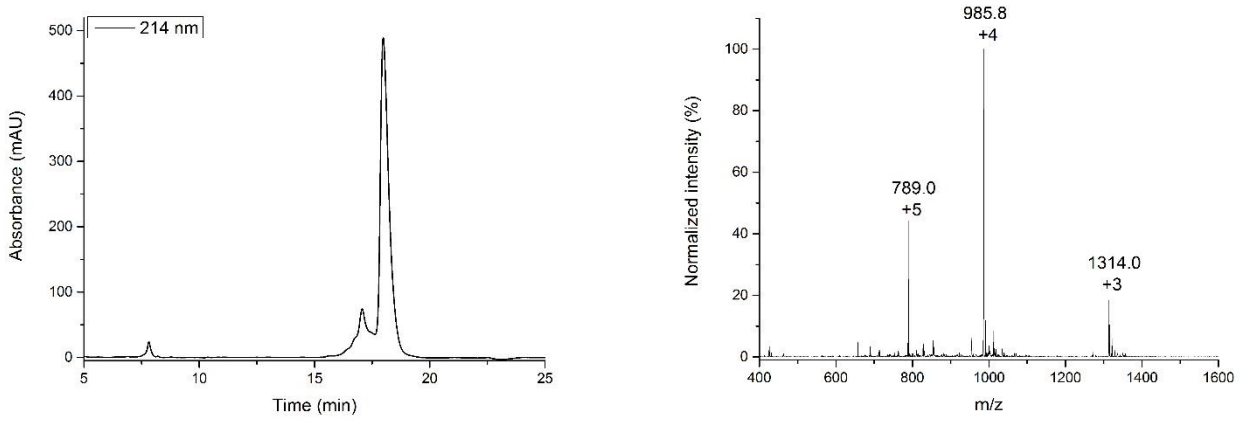

Figure 4-5 **Left:** Analytical UV chromatogram of CC-Pent-Cy5 coupled with HBTU after purification by RP-HPLC. **Right:** ESI-MS of purified CC-Pent-Cy5. Calculated mass for $C_{194}H_{315}N_{42}O_{44}^{+}$: 3939.8 $[M+H]^{+}$. Observed masses: 1314.0 $[M+3H]^{3+}$, 985.8 $[M+4H]^{4+}$, 789.0 $[M+5H]^{5+}$.

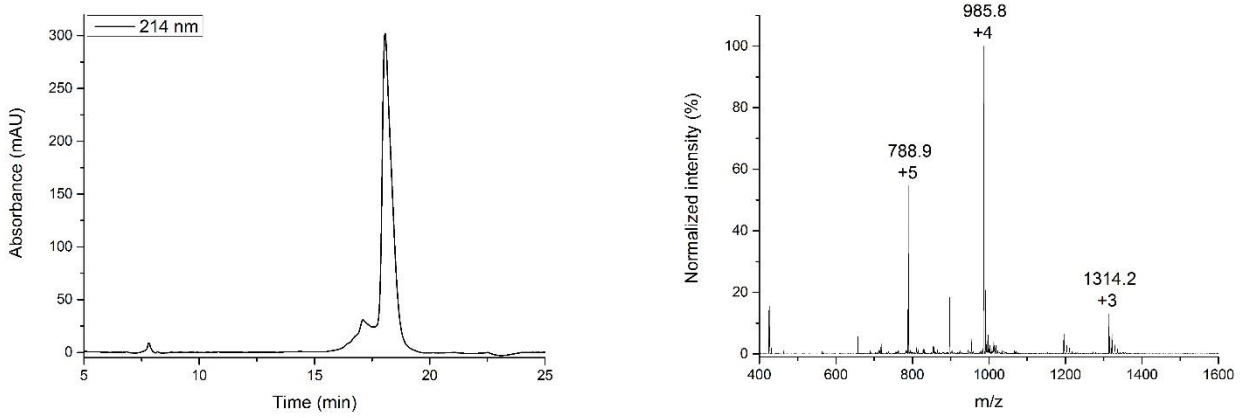

Figure 4-6 **Left:** Analytical UV chromatogram of CC-Pent-Cy5 coupled with Oxyma after purification by RP-HPLC. **Right:** ESI-MS of purified CC-Pent-Cy5. Calculated mass for $C_{194}H_{315}N_{42}O_{44}^{+}$: 3939.8 $[M+H]^{+}$. Observed masses: 1314.2 $[M+3H]^{3+}$, 985.8 $[M+4H]^{4+}$, 788.9 $[M+5H]^{5+}$.

With all three coupling conditions the attachment of Cy5 could be achieved. However, all peptides contained an unidentifiable impurity, which could not be removed during the purification. Since the impurity could not be observed for the unmodified CC-Pent-T, it most likely occurred during the coupling of Cy5. Since a high percentage of the obtained products consisted of the desired peptide and the effect of the impurity is unknown, the

obtained peptides were used for fluorescence microscopy. The peptide syntheses yielded 1.2 mg (6%, HATU), 1.6 mg (8%, HBTU) and 1.2 mg (6%, Oxyma) of CC-Pent-Cy5.

4.1.5 Synthesis of KRRIL

KRRIL was synthesized manually on a 0.005 mmol scale, using the standard Fmoc-SPPS protocol. Presynthesized RRIL on Wang resin was used as solid support. The quality of the synthesis was monitored by test cleavages and Kaiser tests. After the synthesis, cleaving from the support was achieved, using the standard cleavage procedure. The peptide was purified by RP-HPLC (Waters AutoPurification HPLC/MS System, semi-preparative C4 column, 10 mL/min flow rate, 5% to 65% buffer in 40 min). Analytical RP-HPLC runs were performed on a Dionex Ultimate 3000 (analytical C4 column, 1.0 mL/min flow rate, 5% to 65% buffer B in 20 min). The peptide was obtained in high purity and yielded 1.1 mg (33%).

Sequence: H- KRRIL -OH

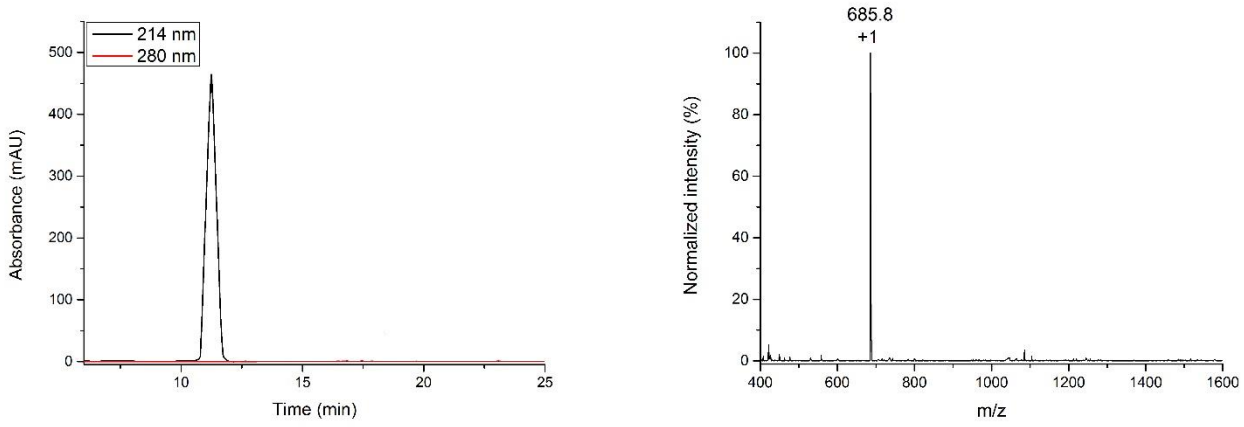

Figure 4-7 **Left)** Analytical UV chromatogram of KRRIL after purification by RP-HPLC. **Right)** ESI-MS of purified KRRIL. Calculated mass for $C_{30}H_{60}N_{12}O_6^+$: 685.9 $[M+H]^+$. Observed mass: 685.8 $[M+1H]^{1+}$.

4.1.6 Synthesis of CC-Hex-T

CC-Hex-T was synthesized automatically on a 0.1 mmol scale, using Fmoc-SPPS on a Liberty Blue microwave peptide synthesizer. Preloaded Fmoc-Glu(OtBu)-TentaGel™-resin (0.19 mmol/g loading) was used as solid support. The quality of the synthesis was monitored by test cleavages. After the synthesis, cleaving from the support was achieved,

using the standard cleavage procedure. The peptide was purified by RP-HPLC (Waters AutoPurification HPLC/MS System, preparative C4 column, 20 mL/min flow rate, 25% to 65% buffer B in 40 min). Analytical RP-HPLC runs were performed on a Dionex Ultimate 3000 (analytical C4 column, 0.3 mL/min flow rate, 25% to 85% buffer B in in 20 min). The peptide was obtained in high purity and yielded 26.2 mg (17%).

Sequence: H- LKAIAQE LKAIAKE LKAIAWE LKAIAQE -OH

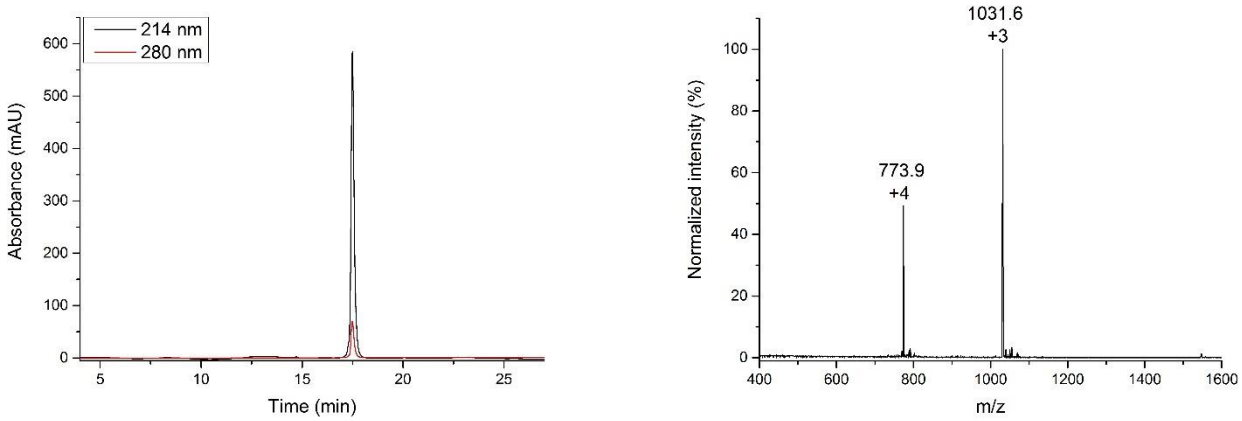

Figure 4-8 **Left)** Analytical UV chromatogram of CC-Hex-T after purification by RP-HPLC. **Right)** ESI-MS of purified CC-Hex-T. Calculated mass for $C_{143}H_{244}N_{36}O_{39}^{+}$: 3092.7 $[M+H]^{+}$. Observed masses: 1031.6 $[M+3H]^{3+}$, 773.9 $[M+4H]^{4+}$.

4.1.7 Synthesis of CC-Hex-Mod-1

The linear part of CC-Hex-Mod-1 was synthesized manually in a 0.1 mmol scale, using the standard Fmoc-SPPS protocol. The N-terminal isoleucine was coupled with a Boc protection group instead of Fmoc. Fmoc-Lys(Mtt)-OH was used for the lysine at the **f** position to enable selective coupling on its side chain. Preloaded Fmoc-Glu(OtBu)-TentaGel™-resin (0.19 mmol/g loading) was used as solid support. The resin was split in half and selective deprotection of the lysine was performed. The remaining KRILL sequence was coupled manually, also following the standard Fmoc-SPPS protocol. The quality of the synthesis was monitored by test cleavages and Kaiser tests. After the synthesis, cleaving from the support was achieved, using the standard cleavage procedure. The peptide was purified by RP-HPLC (Waters AutoPurification HPLC/MS System, semi-preparative C4 column, 10 mL/min flow rate, 25% to 65% buffer B in 40 min). Analytical RP-HPLC runs were performed on a Dionex Ultimate 3000

(analytical C4 column, 1.0 mL/min flow rate, 25% to 85% buffer B 20 min). The peptide was obtained in high purity and yielded 13.2 mg (14%).

Sequence: H- LKAIAQE LKAIAKE LKAIAWE LKAIAQE -OH
KRRIL

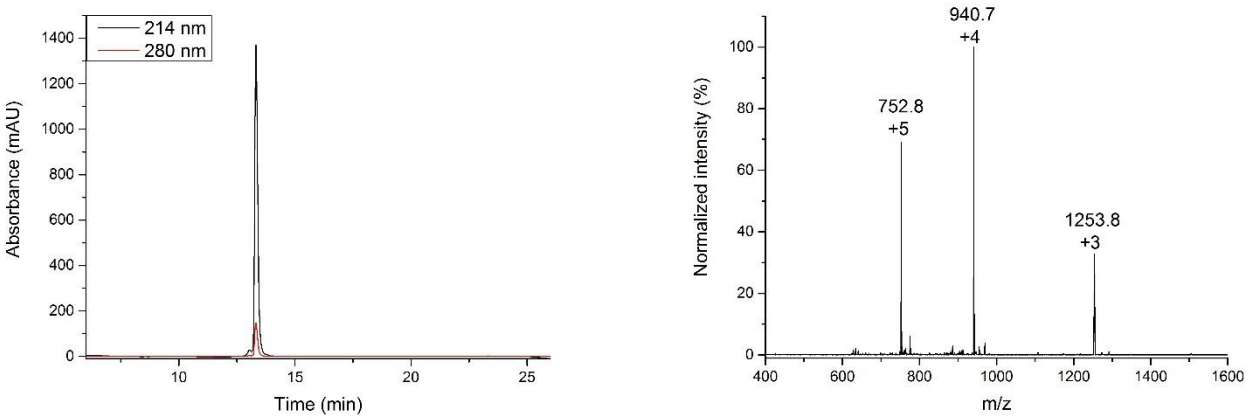

Figure 4-9 Left) Analytical UV chromatogram of CC-Hex-Mod-1 after purification by RP-HPLC. **Right)** ESI-MS of purified CC-Hex-Mod-1. Calculated mass for $C_{173}H_{302}N_{48}O_{44}^{+}$: 3759.6 $[M+H]^{+}$. Observed masses: 1253.8 $[M+3H]^{3+}$, 940.7 $[M+4H]^{4+}$, 752.8 $[M+5H]^{5+}$.

4.2 Characterization of self-assembled peptide nano tubes

To characterize the assembly of the peptides into PNTs, several biophysical and biochemical assays were performed. The first step was to confirm the α-helical structure of the coiled-coil peptides. For this purpose, CD spectra of all peptides were recorded and their secondary structure was determined. Visualization of assembled PNTs was achieved by scanning electron microscopy. To further investigate the presence of an accessible lumen and observe the assembly over time, an assay adapted from Burgess *et al.* was used. Lastly, by using energy dispersive X-ray spectroscopy, it was excluded that silica was present in the peptide samples prior to the *in vitro* precipitation.

4.2.1 Circular Dichroism (CD)

To determine whether the modified versions of the coiled-coil peptides have still a defined α-helical structure, CD spectra were recorded of all peptides, except for CC-Pent-Cy5. For

CC-Hex-T and CC-Pent-T, CD spectra were already obtained by Burgess *et al.* and served as reference. By comparing the data with spectra from the database, the amount of secondary structure elements was calculated afterwards. Since all spectra were recorded in aqueous buffer, a high percentage of α-helices was expected. However, the lack of α-helices could indicate an incorrect folding of the peptide. In this case, the further assemble into ordered peptide nanotubes is highly unlikely.

CC-Pent-T and CC-Hex-T

For CC-Hex-T and CC-Pent-T spectra with helical characteristics were obtained. Both peptides showed the typical local minima at 208 nm and 222 nm (Fig. 4-10). Similar spectra were also reported by Burgess *et al.* under the same conditions. This would indicate a proper folding of the peptides, required for the coiled-coil motif and its further assembly. However, using this data to calculate the secondary structure elements showed deviations from the spectra (Tab. 4-2). With 83.7%, CC-Pent-T had the expected high percentage of helices. Though, for CC-Hex-T only 30.8% of the peptide was helical and a higher amount was consisting of random coils. Since all spectra were recorded in two different setups and Burgess *et al.* obtained similar spectra, technical defects can be excluded. Furthermore, the obtained spectrum showed the distinct characteristic of helices, which still indicates a helical structure of CC-Hex-T.

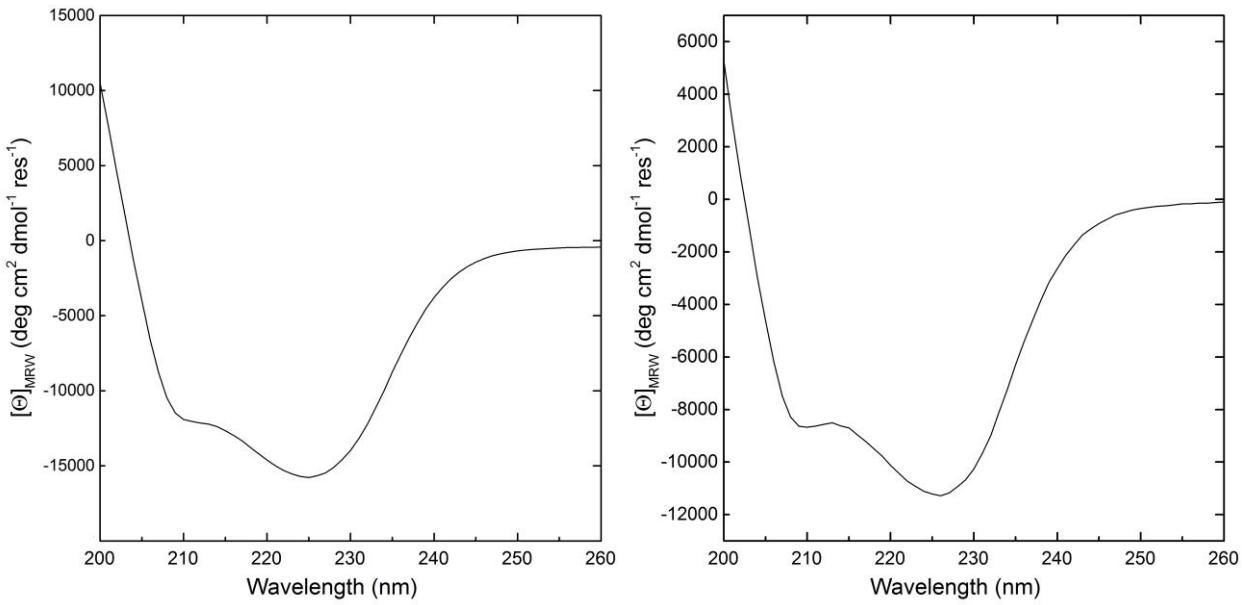

Figure 4-10 CD spectra of CC-Pent-T (left) and CC-Hex-T (right). Spectra were recorded at room temperature, in PBS buffer and at a concentration of 0.1 M.

Table 4-2 Percentage of secondary motifs in CC-Pent-T and CC-Hex-T. Calculations were performed using CDNN software and normalized.

	CC-Pent-T	CC-Hex-T
Helix	83.7	30.8
Antiparallel	0.0	5.1
Parallel	2.1	11.0
Beta-turn	3.7	15.1
Random Coil	10.6	37.9

KRRIL

To estimate the influence of the KRRIL structure on the coiled-coil peptides, a CD spectrum of KRRIL was recorded as well. Depending on its secondary structure, possible predictions for the modified peptides can be made. Since its secondary structure has not been investigated yet, an evaluation using spectra interpretation software was performed. Similar to CC-Pent-T and CC-Hex-T, the KRRIL sequence showed characteristic minima at 208 and 222 nm (Fig. 4-11). However, comparing the spectra of CC-Pent-T, CC-Hex-T or α-helical peptides with the KRRIL sequence showed several differences. The main variation was the ratio between the two minima at 208 and 222 nm. Both unmodified peptides exhibited their lowest ellipticity at 222 nm, whereas the KRRIL tag displayed it at 208 nm. Nevertheless, using the CDNN software to calculate the secondary motifs revealed, that around 92% of the tag still resemble helices. (Tab. 4-3) Since both the coiled-coil peptides and the KRRIL tag had helical structures, the modified versions should also carry a high percentage of helical structure elements.

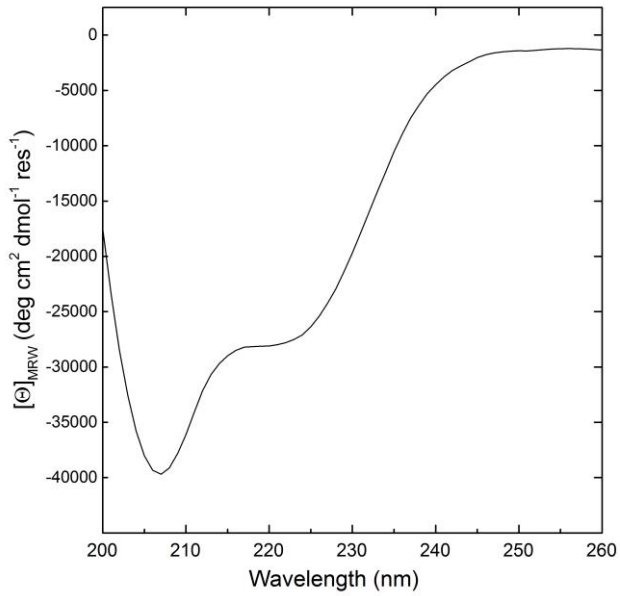

Figure 4-11 CD spectrum of the KRRIL sequence. The spectrum was recorded at room temperature, in PBS buffer and at a concentration of 0.1 M.

Table 4-3 Percentage of secondary motifs in the KRRIL sequence. Calculations were performed using CDNN software and normalized.

	KRRIL
Helix	91.8
Antiparallel	0.6
Parallel	0.0
Beta-turn	7.3
Random Coil	0.3

CC-Pent-Mod-1 and CC-Pent-Mod-2

Helical characteristics were also exhibited in the CD spectra of CC-Pent-Mod-1 and CC-Pent-Mod-2 (Fig. 4-12). Both peptide spectra displayed the typical minima at 208 and 222 nm. However, comparing the data from the unmodified peptides with the modified versions revealed several differences. The minima of ellipticity shifted from 222 nm to 208 nm. This feature could also be found in the spectrum of the KRRIL sequence. Furthermore, a linear combination of the KRRIL spectrum with the CC-Pent-T spectrum displayed similar data as the obtained spectra. This could indicate that neither the coiled-coil peptide nor the attached moiety experienced a loss in their secondary structure by the

coupling. The software calculation for the percentage of secondary motifs showed consistent results for CC-Pent-Mod-1. 83.7% of the peptide displayed helical structure, which is the same as for the unmodified peptide (Tab. 4-4). Yet, for CC-Pent-Mod-2, which has two KRILL moieties attached, a decreased percentage of helical elements was calculated (72.9%). This decrease is either due to the additional attached KRRIL or due to the impurification. The extra positive charges introduced by the lysine of the KRRIL tag could have influence on the folding of the peptide. A second possibility is the lysine, which replaces the glutamic acid. Since no data are present for an unmodified coiled-coil peptide with this sequence, it cannot be excluded that the lysine has influence on the helical folding. However, it is more likely that the decrease is caused by the impurity. Because a small fraction of the peptide was lacking a glutamic acid in its sequence, it is expected that deviations from a purified peptide are present. The lacking amino acid disturbed most probably the heptad repeat and subsequently proper folding of the peptide, which resulted in an increased percentage of random coils.

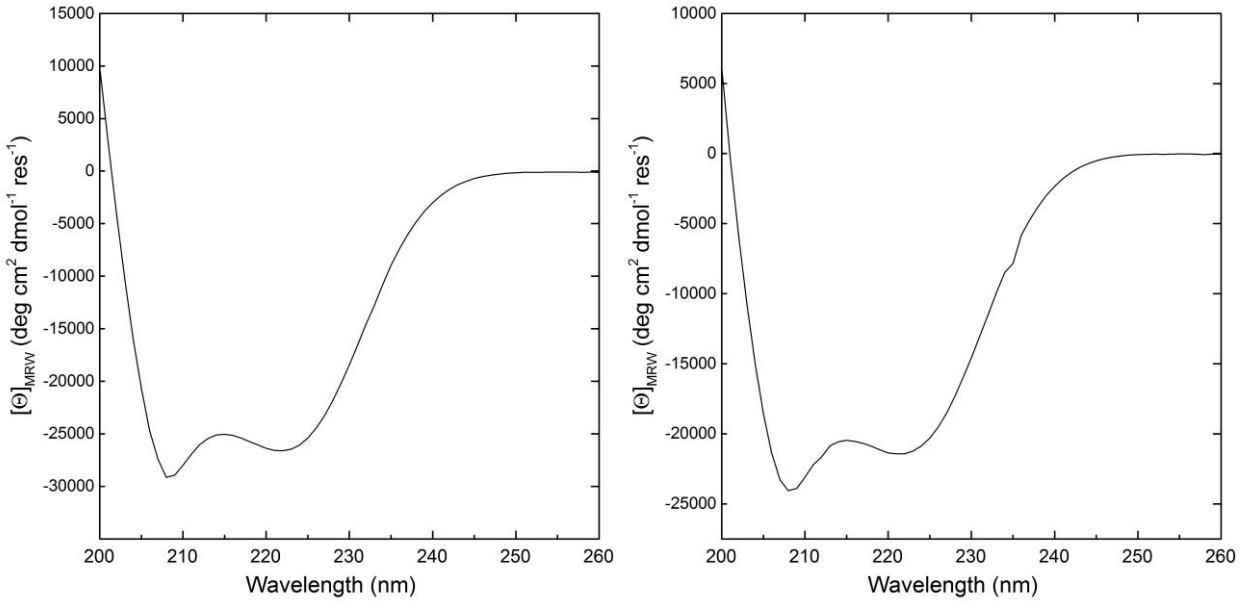

Figure 4-12 CD spectra of CC-Pent-Mod-1 (left) and CC-Pent-Mod-2 (right). Spectra were recorded at room temperature, in PBS buffer and at a concentration of 0.1 M.

Table 4-4 Percentage of secondary motifs in CC-Pent-Mod-1 and CC-Pent-Mod-2. Calculations were performed using CDNN software and normalized.

	CC-Pent-Mod-1	CC-Pent-Mod-2
Helix	83.7	72.9
Antiparallel	0.6	1.9
Parallel	1.3	2.2
Beta-turn	9.6	12.7
Random Coil	6.5	10.3

CC-Hex-Mod-1

The obtained spectrum of CC-Hex-Mod-1 resembled the spectrum of the unmodified peptide (Fig. 4-13). The same minima could be overserved, indicating a percentage of helical elements in the secondary structure. However, the shift of the minima to 208 nm, which was observed for the modified versions of the pentamer, was not present. On the contrary, the minima at 208 nm was even less distinct. This deviated from the expected spectrum, which could be obtained in the case of the pentamers. Using the spectrum to calculate the secondary structure motifs revealed a decreased amount of helices in the peptide (Tab. 4-5). With only 13% a loss of 17% occurred. Analogue to the unmodified hexamer, a high percentage of random coils could be observed again (42.5%). Since the unmodified hexamer had already a high amount of random coils, a similar result was expected. However, the presence of only 13% helical elements could indicate a further loss in the secondary structure of the peptide.

Table 4-5 Percentage of secondary motifs in CC-Hex-Mod-1. Calculations were performed using CDNN software and normalized.

	CC-Hex-Mod-1
Helix	13.3
Antiparallel	13.4
Parallel	15.2
Beta-turn	15.6
Random Coil	42.5

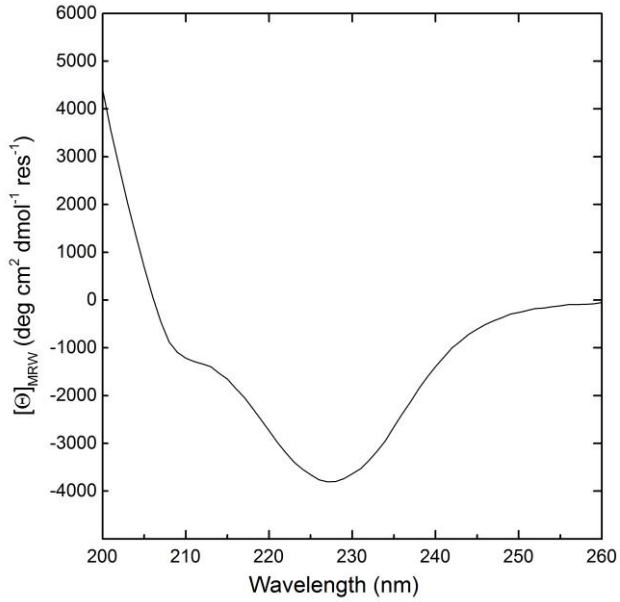

Figure 4-13 CD spectra of CC-Hex-Mod-1. The spectrum was recorded at room temperature, in PBS buffer and at a concentration of 0.1 M.

4.2.2 Scanning electron microscopy

To visualize assembled PNTs, samples of all peptides for scanning electron microscopy were prepared. All peptides were dissolved in PBS buffer and incubated at room temperature for at least 72 h to give the peptide sufficient time to assemble. The dissolved peptides were applied on a plastic coverslip and given 5 min to adsorb on the surface. The buffer was removed and the coverslip washed to prevent salts of the buffer on the sample.

Table 4-6 Used sample preparation conditions for KRILL-modified and unmodified peptides.

	Concentration (mM)	**Incubation time on coverslip (min)**	**Washing steps**
1	0.1	5	2
2	0.2	5	2
3	0.5	5	2
4	0.1	10	2
5	0.1	30	2
6	0.1	5	1
7	0.1	5	0

Unexpectedly only for CC-Pent-T fiber formation could be observed (Fig. 4-15). Neither for CC-Hex-T nor for the modified peptides PNTs could be identified, even under different sample preparation conditions (Tab. 4-6). For the modified peptide several possible reasons exist why no fiber formation could be observed by SEM. Assembly of the fibers is mainly driven by the opposite charges at the end of the coiled-coils. By introducing an additional sequence, with several positively charged side chains, the charge dependent assembly might be disturbed. A second possible explanation is the size of eventually assembled tubes. Since the KRRIL sequence is attached on the outer surface of the coiled-coil, a lateral assembly of the tubes is prevented. Therefore, a thickening of the peptide fibers is not possible. Formed single fibril chains might be too small to be detected by SEM. Changing to methods with higher resolution, like TEM, could possibly help to visualize the single stranded PNTs.

The fact, that no PNTs could be observed for CC-Hex-T, is contradicting the work of Burgess *et al.*. [23] Several of their studies demonstrated a highly ordered assembly of the peptide under identical conditions. Switching to different concentrations, incubation times or washing steps led in no case to detectable peptide fibers (Tab. 4-6). In a few samples, occasional fiber-like structures could be found. However, these fibers were rare and didn't match the morphology of the PNTs Burgess *et al.* described. Since the ESI-MS data showed the correct mass of the peptide, missing amino acids or impurities can be excluded.

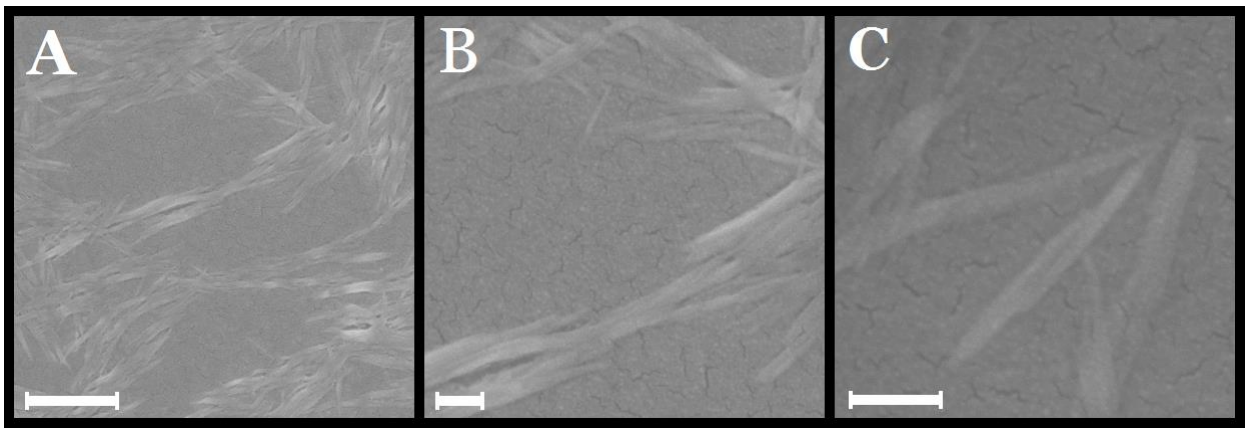

Figure 4-15 Electron micrographs of assembled peptide nanotubes of CC-Pent-T at different magnifications. Scale bars: A) 1 µm, B) and C) 200 nm.

Furthermore, the similarity of the obtained CD spectrum with existing data of Burgess *et al.* provides further proof of the correct peptide. [23] The use of a scanning electron

microscope instead of a TEM, which was used in the reference, could interfere with the visualization of the nanotubes.

Parallel to CC-Hex-T, samples of CC-Pent-T were investigated. Following the sample preparation of Burgess *et al.* PNTs could be observed consistently. However, the immediate assembly of peptide nanotubes could not be confirmed. For freshly dissolved peptide (< 1 h), no fiber formation could be detected on the electron micrographs. After more than 72 h of incubation at room temperature, fiber formation in the sample could be confirmed. The assembled peptides could be stored at room temperature over several days without further change in morphology, which indicates a highly kinetically stable assembly of the peptide. The size of the peptide fibers length was between 500 and 700 nm, while their diameter ranged between 30 and 40 nm. Assembled fibers were present mainly in clusters due to the increase of peptide concentration during the sample preparation. Similar results, regarding size and morphology of the PNTs, were also reported by Burgess *et al.*.

To obtain nanotubes, with both CC-Pent-T and CC-Pent-Mod-1, different concentration combinations of the peptides were prepared and incubated. Mixtures with 25 µM : 75 µM, 50 µM : 50 µM and 75 µM : 25 µM were prepared and incubated together for 72 h. However, none of the samples yielded detectable nanotubes. Analyzing the supernatant by LC-MS after centrifugation, revealed the presence of both peptides. This proofs the assumption, that the attachment of the KRRIL sequence inhibits the assembly of peptide fibers. Even if unmodified peptide is present in excess, the positive charged side chains influence the assembly in such manner, that the charge dependent assembly is prevented. Lastly, the ability of the KRRIL sequence alone to form ordered structures was investigated. Using the same conditions as for the coiled-coil peptides, no fiber-like structures could be detected. Since a high percentage consist of positively charged amino acids, repulsive interactions will most likely prevent an ordered assembly of the sequence.

4.2.3 Size analysis of nano tubes assembled from CC-Pent-T

The formed peptide nanotubes displayed an average length of 650 nm and an average width of 50 nm (Fig. 4-16). However, this data is slightly deviating from the results of Burgess and coworkers, who measured an average width between 30 and 35 nm. A possible explanation for this discrepancy in width is the used visualization method. Since for the scanning electron microscopy all samples had to be sputtered with gold

beforehand, a small increase in length and diameter is reasonable. The sputtered gold layer was in the range of 5 nm, which would explain the 10 - 15 nm difference in the diameter.

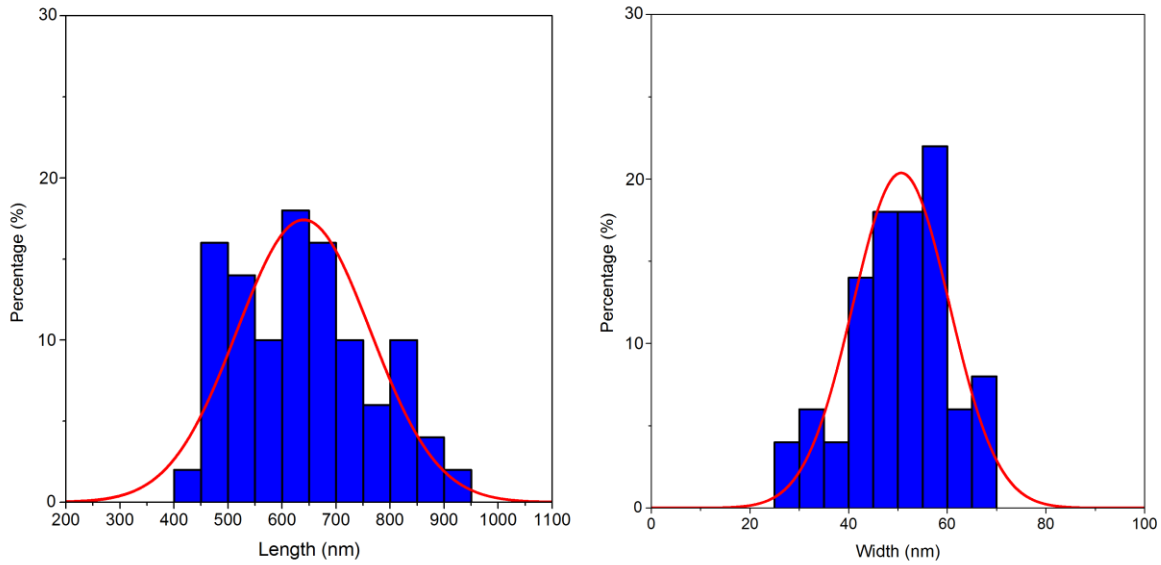

Figure 4-16 Distribution of lengths and widths of CC-Pent-T peptide nanotubes measured from corresponding electron micrographs. The analyzed peptide sample was incubated for at least 72 h with a concentration of 100 µM. Bin sizes are 50 nm and 5 nm respectively. A normal distribution curve was fitted over the obtained histogram.

4.2.4 1,6-diphenyl 1,3,5-hexatrien (DPH) intercalation assay

To investigate the accessibility of the internal chancel of assembled peptide fibers, an assay adapted from Burgess *et al.* was used. [23] The assay is based on the molecule 1,6-diphenyl 1,3,5-hexatrien, which is small enough to be able to intercalate into the lumen of the PNTs. DPH is an environment sensitive dye, which has no fluorescence in aqueous solvents, but has a strong fluorescence at 455 nm in hydrophobic surroundings. By adding low concentrations of the dye to incubated PNTs, the dye intercalates in the lumen of the tubes and fluorescence can be observed. The assay can be used to prove the presence of eventually formed nano tubes, which could not be detected by the SEM.

A high level of fluorescence could be detected for CC-Pent-T, which confirmed the presence of nano tubes (Fig. 4-17). The data verified the actual presence of hollow tubes with accessible lumen instead of only assembled fibers. All obtained data for CC-Pent-T matched the results from Burgess *et al.* and were reproducible. Even for CC-Hex-T fluorescence could be observed in the assay. The fluorescence could indicate that CC-Hex-T assembled into PNTs, but during the sample preparation or during the

microscopy the assembly is lost. However, the fluorescence observed for CC-Hex-T is only 38% of the fluorescence displayed by CC-Pent-T. This might also be caused by an incorrect assembly of the peptide. Weather the visualization method or an impaired assembly of the peptide are the reason for no detectable nanotubes was not further investigated during this work.

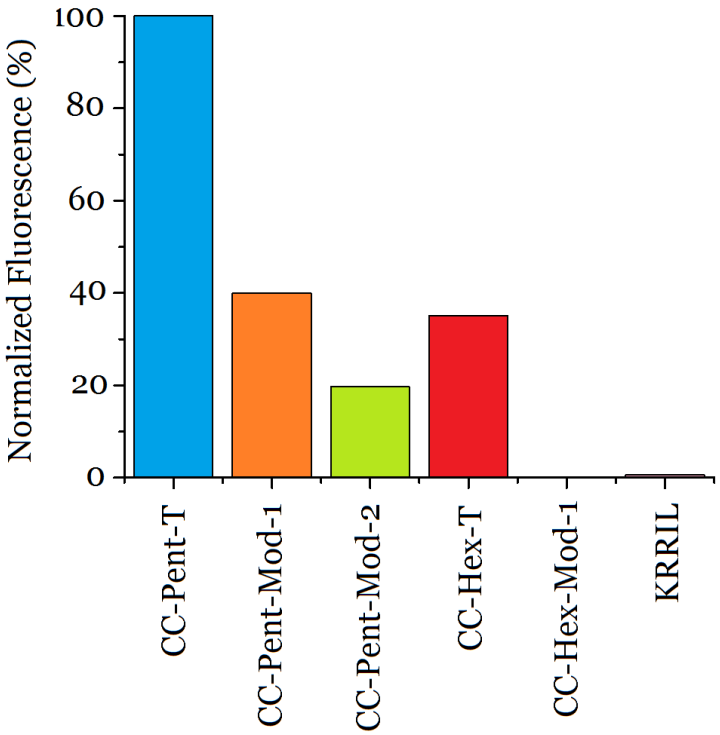

Figure 4-17 Accessibility of the internal lumen of unmodified and modified coiled-coil peptides and the KRRIL sequence to the dye 1,6-diphenyl 1,3,5-hexatrien. λ_{ex} = 350 nm, λ_{em} = 455 nm. Peptides were incubated at room temperature for 72 h before. Data was normalized to the maximal obtained fluorescence of CC-Pent-T. The peptide concentration is in all cases 25 µM.

Similar fluorescence levels as for CC-Hex-T were obtained for the modified pentamer versions, CC-Pent-Mod-1 and CC-Pent-Mod-2. As a conclusion, the attachment of the KRRIL sequence on the coiled-coil peptide leads to a loss of accessible hydrophobic lumen. This conclusion is in line with the fact that CC-Pent-Mod-2, which has two of the sequences coupled, had a further decrease in fluorescence. However, the presence of fluorescence indicates that hydrophobic environments, in which the dye can intercalate, were present in the sample. The alpha-helical barrels might still be able to assemble, because hydrophobic interactions should not be inhibited by the KRRIL tag. The charge dependent stacking of the barrels on the other side could be influenced by the positive

charges of the sequence, which led to an unordered assembly of the barrels and therefore to a decreased fluorescence.

No fluorescence could be detected for the modified CC-Hex-Mod-1. This circumstance was possibly caused by several factors. First of all, the attached KRRIL tag most likely resulted in a decrease in fluorescence similar to the modified versions of the pentamer. Additionally, the small impure fraction of the peptide, which lacked the glutamic acid, could further inhibit the assembly and therefore no intercalation is possible. Summarizing the results from the CD spectrometry, the electron microscopy and the binding-assay, CC-Hex-Mod-1 had no helical secondary structure, did not assemble into detectable nano tubes and did not form assemblies with hydrophobic lumen.

To exclude that fluorescence is caused by the attached KRRIL sequence, KRRIL was analyzed independently as well. The observed fluorescence (< 3%) is insignificantly small and most likely caused by measuring inaccuracy, which indicates that KRRIL provides no hydrophobic environment for the DPH.

4.2.5 Time resolved assay

The immediate formation of peptide nanotubes, described by Burgess *et al.*, could not be confirmed during the previous experiments. For this reason, all peptide samples were incubated for at least for 72 h after dissolving, before further investigation. To study a time resolved assembly of CC-Pent-T and CC-Hex-T, the binding-assay with DPH was used. Freshly dissolved peptides were immediately mixed with the dye and their fluorescence was observed over a period of 18 h.

Several information regarding the assembly of CC-Pent-T could be obtained from the data (Fig. 4-18). CC-Pent-T, which has been incubated for at least 72 h in PBS, displayed a fluorescence maximum around 3 h after the dye was added. Additionally, a high starting fluorescence could be observed. The 3 h interval is most likely the time, which the DPH needed to intercalate into the PNTs. After the maximum of fluorescence was reached, a rapid decrease in fluorescence was observable, presumably induced by photo bleaching. Freshly dissolved CC-Pent-T showed a different behaviour with a maximum at 10 h after the sample preparation. This proofs, that the peptide did not assemble immediately, like stated by Burgess et al., but rather took several hours for its assembly. A low fluorescence at 0 h displayed the nearly complete absence of PNTs. In the time interval between 6 h and 12 h almost no change in fluorescence occurred. During this time an equilibrium between the formation of nano tubes with the dye intercalation and photo bleaching

transpired. After this period, photo bleaching dominated and a decrease in fluorescence occurred. The assembly of the nanotubes can also be observed with the naked eye. Clouding of the peptide solution happened after 3 h and increased with time. After some hours, the clouding precipitates and could not be dissolved in the buffer.

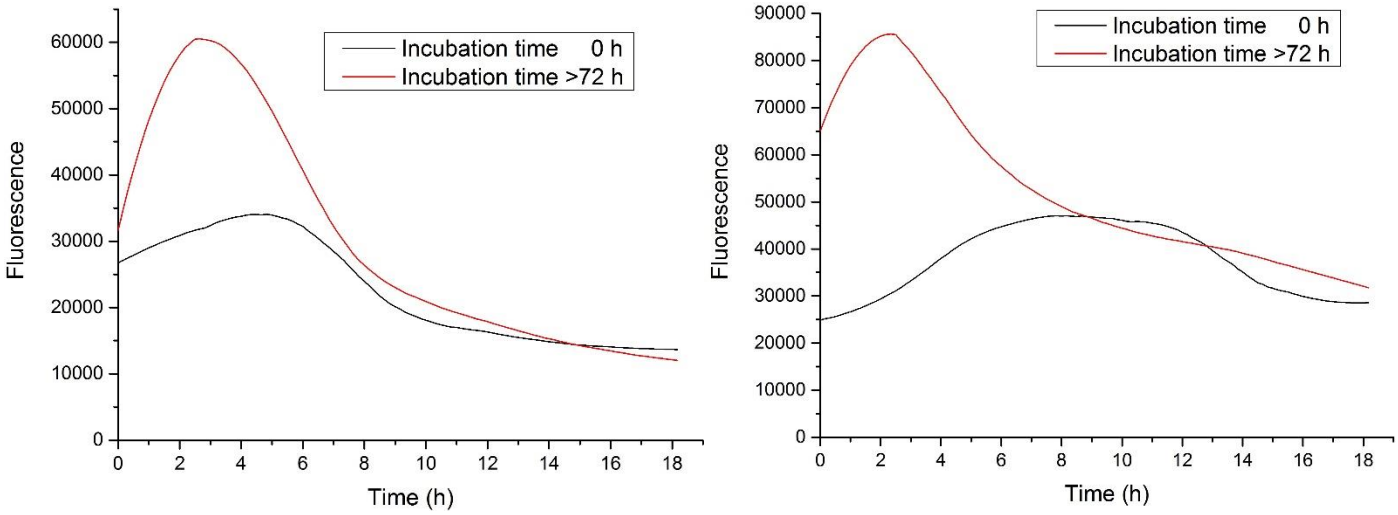

Figure 4-18 Time resolved binding-assay of the assembly of CC-Pent-T (right, 12.5 µM) and CC-Hex-T (left, 50 µM). Compared are freshly dissolved peptides (black line) and preincubated peptide samples (red line) at the same concentration.

For preassembled CC-Hex-T, similar data as for CC-Pent-T was obtained. The maximum of fluorescence was again around 3 h after the dye was added to the peptide. This highlights again the necessary time for the DPH to intercalate into the nano tubes. Fluorescence at 0 h proofs the presence of PNTs when the dye was added. After the maximal fluorescence is reached, photo bleaching led to a rapid decrease in intensity. Different to CC-Pent-T, the fluorescence maxima of newly dissolved CC-Hex-T occurred earlier at 5 h after addition of the dye. Fluorescence at the beginning also hints towards formed nano tubes. This might indicate, that CC-Hex-T assembled faster than CC-Pent-T. Clouding of the sample could already be observed several minutes after the peptide was dissolved. The data from the binding-assay and the visual observations indicate a fast assembly of CC-Hex-T, which happens during the first hours after dissolution of the peptide.

4.2.6 Energy-dispersive X-ray spectroscopy (EDX)

To obtain silica nano tubes, all peptides were tested in silica precipitation experiments. To exclude the presence of any traces of silica in the peptide samples, energy-dispersive

X-ray spectroscopy was performed. Using EDX allows qualitative assertions about the presence of elements in the sample.

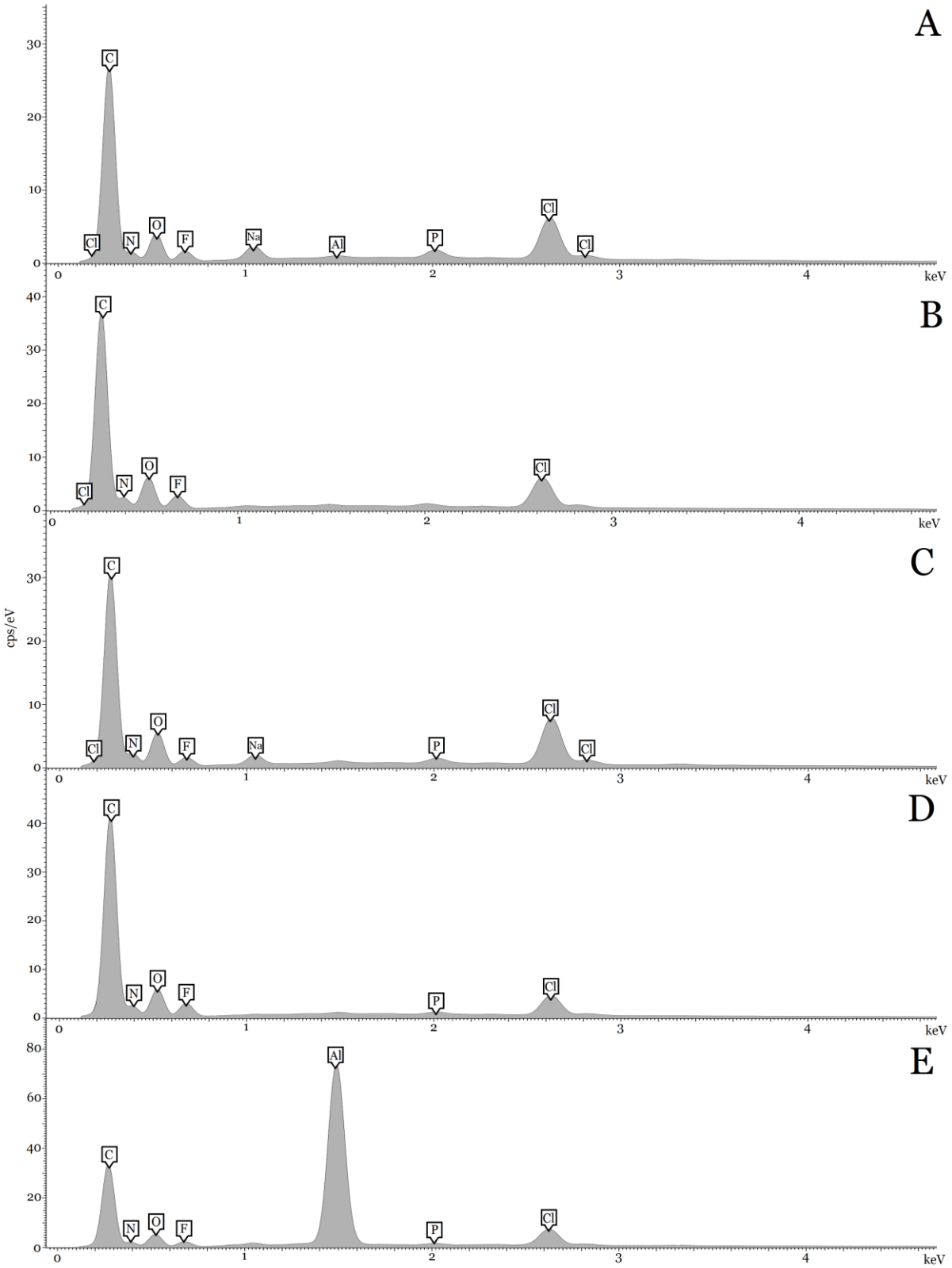

Figure 4-19 EDX analysis of unmodified and modified coiled-coil peptides to exclude the presence of silica. A) CC-Pent-T, B) CC-Pent-Mod-1, C) CC-Pent-Mod-2, D) CC-Hex-T, E) CC-Hex-Mod-1

The EDX analysis confirmed that no silica is present in any of the dissolved peptide samples (Fig. 4-19). The observed elements are either from the peptide itself (C, N, O), PBS buffer (P, Cl, Na), TFA (C, F) or from the sample stopper (Al). Therefore, if silica can be detected in further experiments, it can be excluded that it originates from either the PNTs or PBS buffer.

4.3 Functionalization of coiled coil nano tubes

In diatoms silaffins possess the ability to form highly symmetric silica structures through precise silica depositions. By using synthetic silaffins, this silica precipitation can be mimicked *in vitro*. However, synthetic silaffins lack the guided precipitation of the silica, which can be found *in vivo*, and mainly spherical particles can be observed. The self-assembling of the peptide is suspected to serve as template for the initiation of silica deposition. By functionalizing peptide nanotubes with a short sequence, which is derived from silaffins, it is attempted to achieve a silica precipitation guided by the PNT.
Data from the previous experiments indicated, that the KRRIL sequence most likely disturbed the assembly of the coiled-coil peptide, which prevented an assembly into further nano tubes. However, it has been demonstrated by Burgess *et al.*, that once assembled, PNTs are kinetically stable structures. To prevent the interference of the KRRIL sequence on the assembly, unmodified PNTs were incubated beforehand. By adding different amounts of the functionalized peptide afterwards, the modified peptides should attach on the surface of the PNTs. This would result in peptide fibers, whose core consists of the unmodified PNT and have a shell of KRRIL modified peptide. A subsequent silica precipitation should allow a targeted deposition of silica all around the peptide fiber. To investigate how the KRRIL sequence behaves attached to the various peptides and if a precipitation is even possible, precipitations were performed with all peptides independently and with different combinations.

4.3.1 Silica precipitation with KRRIL-modified and unmodified peptides

CC-Hex-T, CC-Hex-Mod-1

To observe the formed particles of the silica precipitation, scanning electron microscopy was performed. All unmodified coiled-coil peptides, as well as the KRRIL sequence, displayed observable particles after the precipitation (Fig. 4-20). For CC-Hex-T clustered

structures, which consisted of merged fiber-like smaller particles, were noticed (Fig. 4-20; A, B, C). These fiber-like structures had strong resemblance with the fibers, which could be detected occasionally in the dissolved peptide sample. Since extensive washing steps were performed with the particles, the observed structures can't consist of peptide nanotubes only, since PNTs would disassemble during the washing. This indicates that the observed particles were most likely formed during the precipitation. Because no silaffin was attached to the peptide, it can be assumed that a condensation of silicic acid on the surface of the peptide occurred. Silicic acid is known to condensate under acidic or basic conditions, forming a colloid consisting of amorphous spherical particles. However, for the nanotubes the silica was deposited mainly on the surface of the peptide, leading to PNTs covered with a thin film of silica. Using organic matrices in combination with TMOS to obtain silica particles has been already reported elsewhere and is not goal of this work. [54] However, this form of silica deposition is not actively driven by the peptide, which is the case for silaffins.

CC-Hex-Mod-1 displayed the distinct ability to precipitate silica out of silicic acid, which could even be monitored with the naked eye. However, the observed precipitate lacked a defined shape and morphology (Fig. 4-20; D, E, F). The particles slightly resembled merged and deformed spherical particles, which could hint towards a similar behavior as synthetic silaffins. Silica nanotubes could not be detected. Since previous data indicated that an assembly of the peptide into nanotubes is unlikely, chances to obtain silica nanotubes were low. Nevertheless, one important result can be concluded from the precipitation: The attachment of the KRRIL sequence to the side chain of a peptide does not inhibit its activity to precipitate silica.

Obtained particles from CC-Pent-T displayed similar characteristics as its peptide nanotubes. Fiber-like particles, which are nearly homogenous in diameter and length, were the result after silicic acid was added (Fig. 4-20; G, H, I). Silicification induced by the condensation of silicic acid, which could already be observed for CC-Hex-T, was most likely the cause for a thin silica sheath. Using different solvents for the incubation of the coiled-coil peptides, it is known that the peptide disassembles after exposure to ddH_2O. Therefore, it is excluded that observed structures are the result from the peptide alone, since the precipitate was washed several times.

For CC-Pent-Mod-1, a high percentage of spherical particles could be observed (Fig. 4-20; J, K, L). Nevertheless, large assemblies resembling merged spheres were also present in the sample. The similarity of the shape to particles from synthetic silaffins indicates a self-assembly of the peptides before, which Kröger *et al.* postulated for the silaffins. [39] Hence,

interaction of the coiled-coil peptides to larger assemblies can be assumed. This would confirm the theory, that the KRRIL sequence inhibited the assembly of the peptide into nano tubes, but interactions caused by the hydrophobic and charged groups were still present. Since no data to the interactions of the KRRIL motif are available, it cannot be anticipated how its assembly influenced the morphology of the observed particles.

Analogue to CC-Pent-Mod-1, spherical particles were obtained after the precipitation with CC-Pent-Mod-2 (Fig. 4-20; M, N, O). A slight increase in the average diameter was most likely caused by the additionally attached KRRIL sequence. Nevertheless, no silica nano tubes could be detected.

This leads to the conclusion, that the attachment of the KRRIL sequence to the coiled-coil peptides does not result in silica nanotubes without further modification. The modified peptides can actively precipitate silica out of a solution of silicic acid, but due to a presumable disturbed assembly of the peptides or interactions of the KRRIL motif, mainly spherical particles are obtained. Nevertheless, the morphology of the precipitated silica highly indicates that interactions of the peptides are present.

Precipitate from the unattached KRRIL sequence lacked any defined shape and morphology (Fig. 4-20; P, Q, R). This confirms the theory, that the interactions of the coiled-coil peptides are mainly responsible for the shape of the spherical particles. The KRRIL sequence consists only of positively charged and hydrophobic amino acids, which makes it unlikely to have ordered interactions of the peptide. Therefore, the idea to combine a peptide with an ordered assembly and the KRRIL sequence to obtain particles with a desired shape seems feasible. However, it is necessary that the KRRIL sequence does not disturb the assembly of the peptide. A possible solution would be the covalent coupling of the peptides by synthesis after assembly of the PNTs. This would circumvent the problems, caused by the disturbed interactions of the KRRIL sequence.

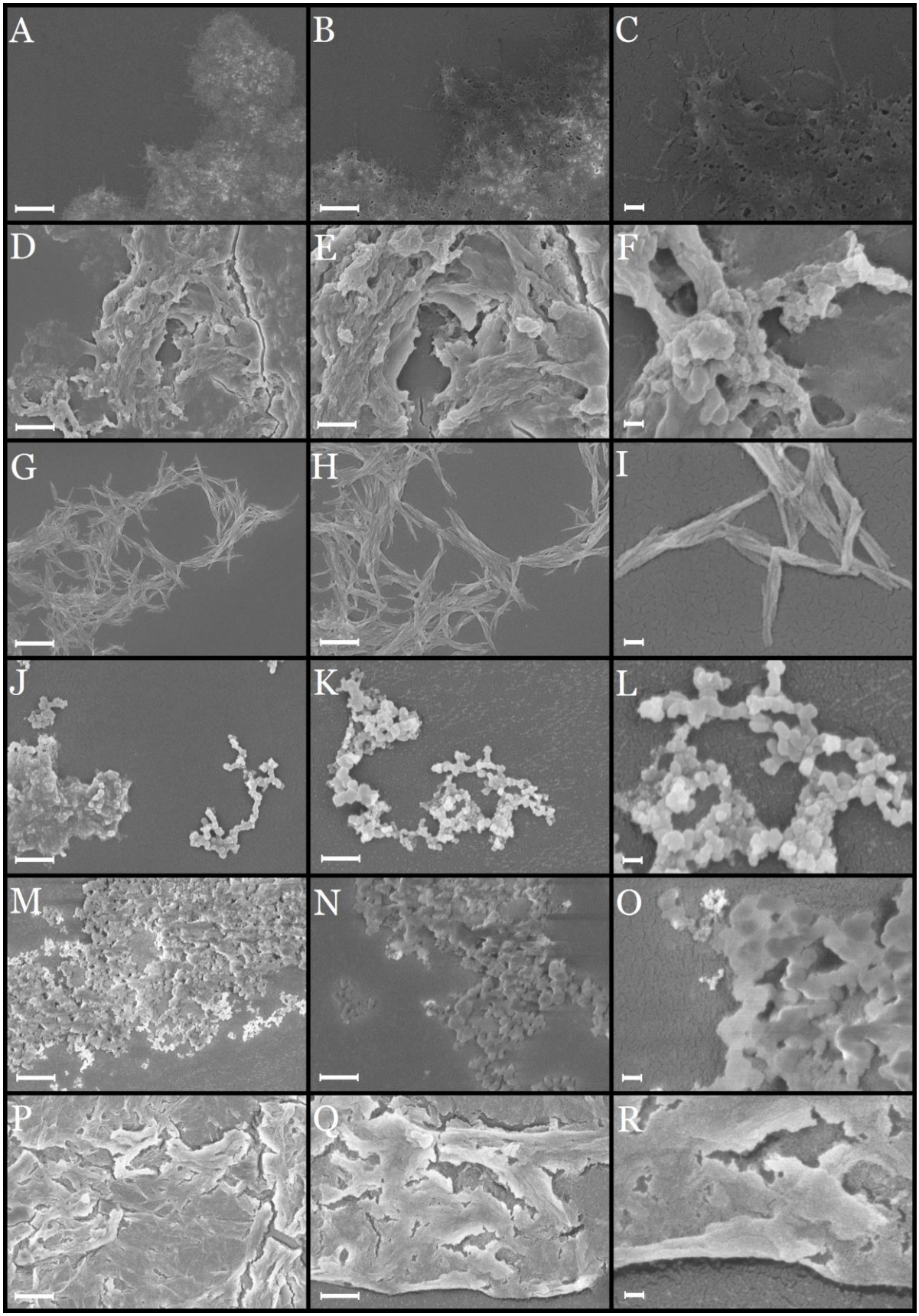

Figure 4-20 Electron micrographs of particles obtained after *in vitro* silica precipitation using CC-Hex-T (A, B, C), CC-Hex-Mod-1 (D, E, F), CC-Pent-T (G, H, I),

CC-Pent-Mod-1 (J, K, L), CC-Pent-Mod-2 (M, N, O) and KRRIL (P, Q R). Scale bars: 2 µm (A, D, G, J, M, P), 1 µm (B, E, H, K, N, Q), 200 nm (C, F, I, L, O, R)

An attempt to bypass the effect of the disturbed assembly with the KRRIL modified CC-Pent-T was carried out, by incubating the unmodified versions of the peptides first at room temperature for at least 72 h to give them time to assemble into PNTs. Afterwards, the modified peptide was added at different concentrations. To observe the effect on the precipitated silica three different variations of peptide concentrations were used (75 µM CC-Pent/Hex-T : 25 µM CC-Pent/Hex-Mod-1/2, 50 µM, CC-Pent/Hex-T : 50 µM CC-Pent/Hex-Mod-1/2, 25 µM CC-Pent/Hex-T : 75 µM CC-Pent/Hex-Mod-1/2).
Even having the third of the concentration of modified CC-Hex-T in the sample resulted in massive changes in the morphology of the precipitate (Fig. 4-21; A, B, C). The precipitate displayed thickened silica fibers, which were merged to large clusters (Fig 4-21; A, B). Structures, resembling fused deformed spherical particles, could also be observed in the sample (Fig 4-21; C). This indicates, that the formed particles inherit characteristics from both peptides. The thickening was most probably caused by deposited silica on the surface of the peptide fibers by the functionalized CC-Hex-Mod-1. Modified peptide, which did not interact with the CC-Hex-T fibers, precipitated silica in the same manner as without CC-Hex-T in the sample. This could already point out, that a third of the amount of modified peptide is sufficient to cover the fibers with silica.
Using equal concentrations of modified and unmodified hexamer further increased the amount of silica clusters with no defined shape (Fig. 4-21; D, E, F). In between the aggregated particles, silica covered peptide fibers could still be detected. However, the diminishing appearance of the fibers displays the results of a higher concentration of the modified peptide. The formed particles resembled more the precipitated silica obtained from CC-Hex-Mod-1 alone. Excess modified peptide, which did not attach to the assembles nanotubes, was most likely again the cause for this form of precipitation.
The particles obtained from a subsequent increased concentration of CC-Hex-Mod-1 displayed none of the characteristics of CC-Hex-T (Fig. 4-21; G, H, I). The precipitated silica lacked any defined shape and did not contain fiber-like structures anymore. The obtained particles beared again close similarities to the precipitate from CC-Hex-Mod-1.
Summarizing the observations from this set of *in vitro* precipitations, low concentrations of modified hexamer lead to thickened silica fiber-like particles. Increasing the concentration of CC-Hex-Mod-1, leads presumable to assembled peptides, which do not interact with the preassembled fibers and whose precipitate exhibits characteristics from

CC-Hex-Mod-1. As soon as a certain concentration of excess modified peptide is reached, no silica fibers can be detected anymore.

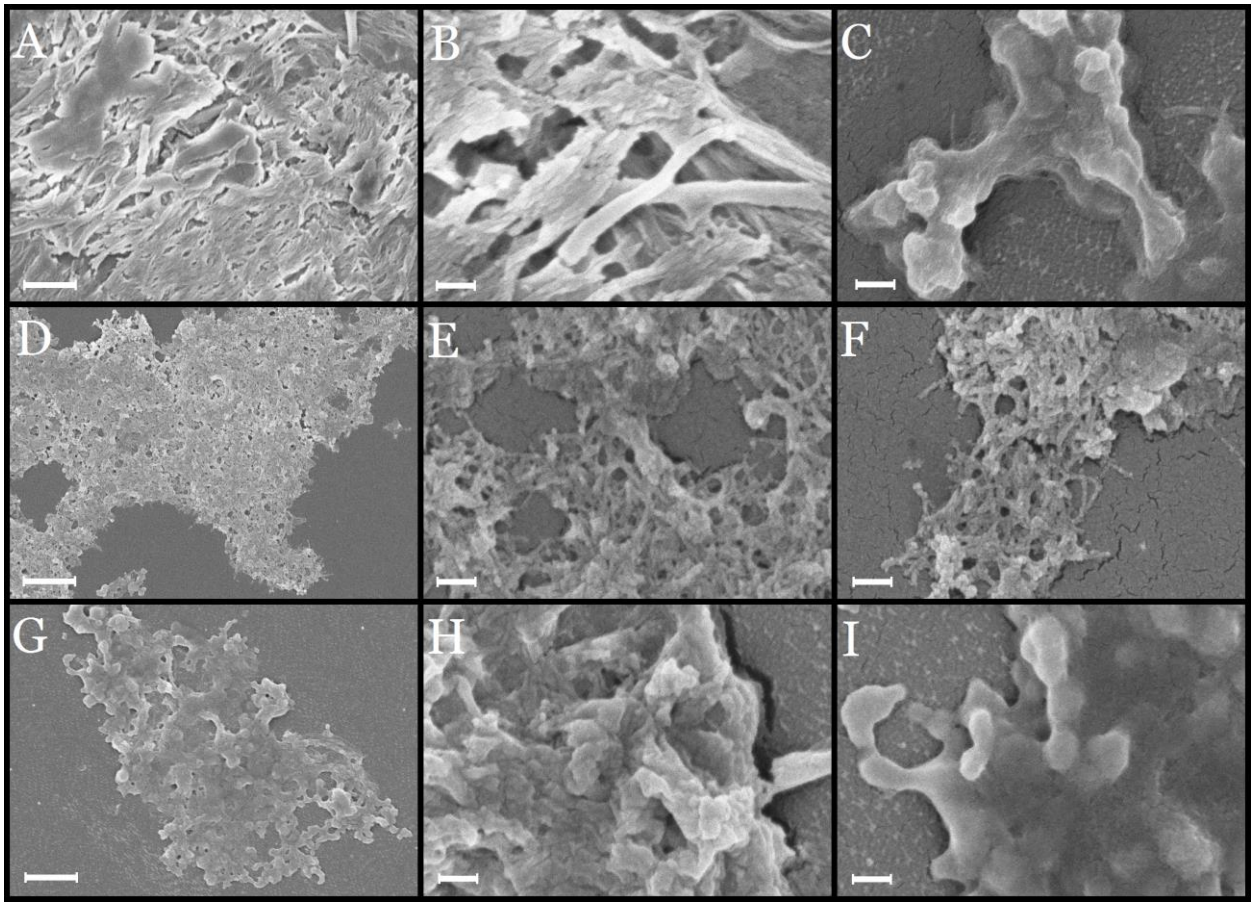

Figure 4-21 Electron micrographs of particles obtained after *in vitro* silica precipitation using different concentrations of CC-Hex-T and CC-Hex-Mod-1: 75 µM CC-Hex-T + 25 µM CC-Hex-Mod-1 (A, B, C), 50 µM CC-Hex-T + 50 µM CC-Hex-Mod-1 (D, E, F), 25 µM CC-Hex-T + 75 µM CC-Hex-Mod-1 (G, H, I). Scale bars: 1 µm (A, D, G), 300 nm (B, C, E, F, H, I).

CC-Pent-T, CC-Pent-Mod-1, CC-Pent-Mod-2

Having a third of the concentration of CC-Pent-Mod-1 in the sample, resulted in rod shaped silica precipitate (Fig. 4-22; A, B, C). In contrast to the observed particles from CC-Pent-T alone, the formed silica exhibited an increased diameter and blunt edges, which both could be results of deposited silica on the surface of the nanotubes. Inhomogeneities in both length and diameter were found in the sample. Additionally, small spherical particles could be observed in addition to the rod-shaped particles. Similar to the hexamer, this was most likely caused by modified peptides, which did not attach to the nanotubes and therefore precipitated silica uncoordinated. Nevertheless, the

altered shape of the precipitate, when nanotubes were added prior to silicic acid, confirms the proposed theory that CC-Pent-Mod-1 attaches to the nanotubes, leading to a coordinated deposition of silica on its surface. The attachment was most likely in a similar matter as the assembly of the peptide nanotubes induced by the linear helical part of the KRRIL-modified peptide. Furthermore, it proves that the addition of the modified peptide after nanotubes assembly does not lead to a detectable disruption of the higher order structures. Therefore, the observed problems with the disturbed assembly can be bypassed by using this method. In addition, the goal of the work to obtain silica nanotubes using the two building blocks was achieved following this procedure.

In the second sample, which had equal concentrations of CC-Pent-T and CC-Pent-Mod-1, similar rod shaped particles could be detected (Fig. 4-22; D, E, F). However, the formed particles displayed a higher inhomogeneity than earlier. Furthermore, the sample exhibited an increased amount of the smaller spherical particles.

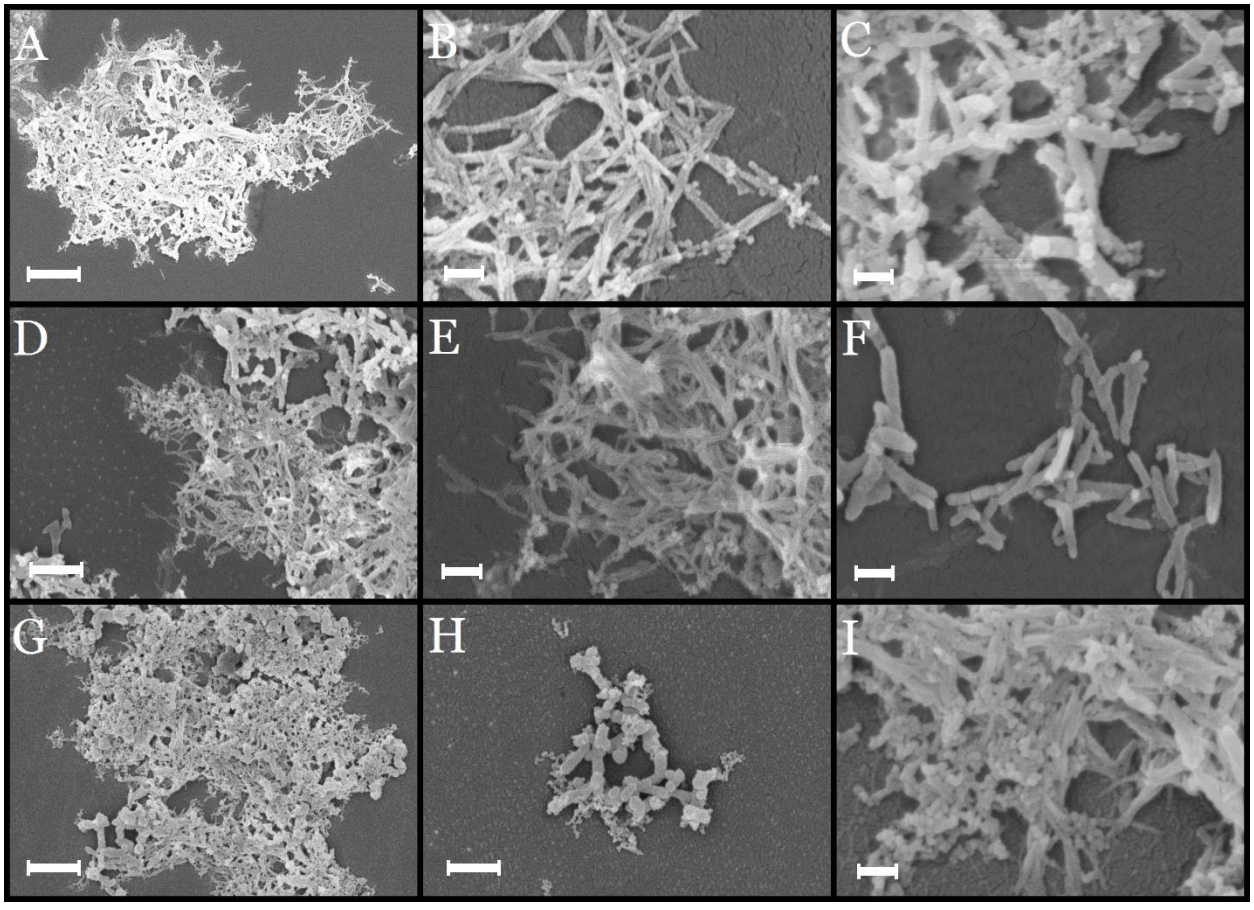

Figure 4-22 Electron micrographs of particles obtained after *in vitro* silica precipitation using different concentrations of CC-Pent-T and CC-Pent-Mod-1: 75 µM CC-Pent-T + 25 µM CC-Pent-Mod-1 (A, B, C), 50 µM CC-Pent-T + 50 µM CC-Pent-Mod-1

(D, E, F), 25 µM CC-Pent-T + 75 µM CC-Pent-Mod-1 (G, H, I). Scale bars: 2 µm (A, G), 1 µm (B, D), 300 nm (B, C, E, F, I).

In the last sample, with the highest concentration of CC-Pent-Mod-1, a further increase of spherical particles was detectable (Fig. 4-22; G, H, I). Additionally, an enhanced amount of thickened and shortened silica rods was present. These results are in line with what could be overserved for CC-Hex-T and CC-Hex-Mod-1. Increasing the amount of modified peptide, increases the characteristics of the particles, which resemble the precipitate of the modified CC-Pent-Mod-1. Furthermore, the more frequent appearance of the spherical particles hints again towards an excess of modified peptide, which did not attach to the nanotubes.

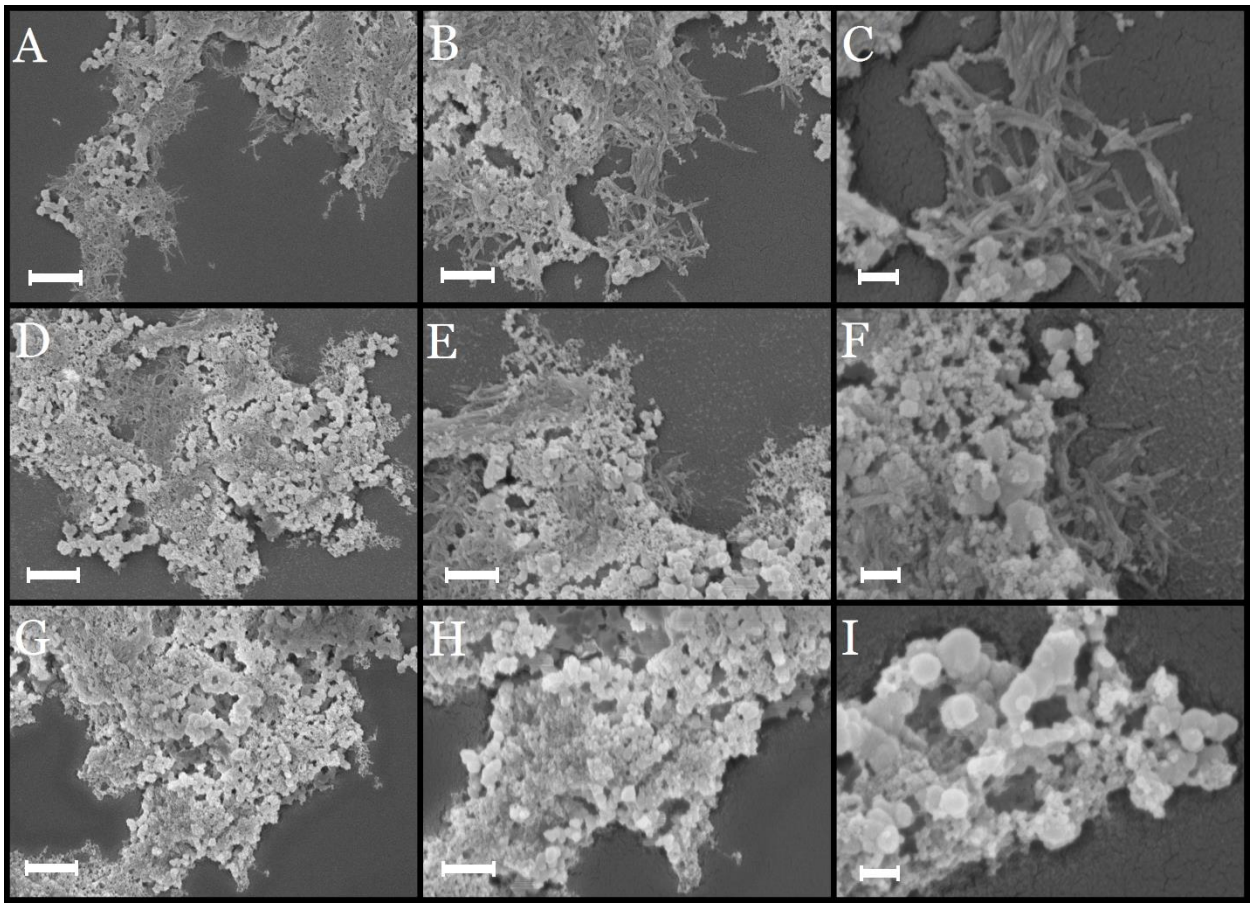

Figure 4-23 Electron micrographs of particles obtained after *in vitro* silica precipitation using different concentrations of CC-Pent-T and CC-Pent-Mod-2: 75 µM CC-Pent-T + 25 µM CC-Pent-Mod-2 (A, B, C), 50 µM CC-Pent-T + 50 µM CC-Pent-Mod-2 (D, E, F), 25 µM CC-Pent-T + 75 µM CC-Pent-Mod-2 (G, H, I). Scale bars: 2 µm (A, D, G), 1 µm (B, E, H), 300 nm (C, F, I).

Samples with CC-Pent-Mod-2 also displayed silica particles with a large inhomogeneity in size and morphology. Even at low concentrations of the modified pentamer, a drastic increase in spherical particles was observable when compared to samples with CC-Pent-Mod-1 (Fig. 4-23; A, B, C). Rod shaped particles, which were present in the sample, appear thinner and less defined. Since CC-Pent-Mod-2 has two KRILL sequences attached on its side chains, interferences caused by the modification are further enhanced. This seems to include an increased attachment to the nanotube surface as well as a disturbed assembly of the peptide, which led to the increase of spherical particles.
Further increasing the concentration of CC-Pent-Mod-2 only resulted in a decrease of rod shaped particles and an increase of spherical particles (Fig. 4-23; D, E, F and G, H, I). These results are in line with previous observations made with the samples containing CC-Hex-Mod-1 and CC-Pent-Mod-1.
The results of these precipitations lead to several conclusions regarding the combined precipitation of modified and unmodified peptide. Adding the modified peptide to the preassembled nanotubes causes the formation of rod shaped particles, as soon as silicic acid is added. Since the modified peptides alone did not display any kind of fiber-like morphology, it can be assumed that once the nanotubes are assembled, the addition of KRILL-modified peptides does not disturb the assembly. Because the silica is mainly deposited on the nanotube surface, the modified peptide most likely attaches to the surface of the PNTs, which leads to a coordinated deposition of silica. A theoretical ideal concentration of modified peptide might exist, which is sufficient enough to cover the peptide nanotubes in a shell of silica (Fig. 4-24). Using lower amounts of modified peptide, most likely result in a decreased deposition of silica on the surface. However, this is still not verified and has yet to be demonstrated. A further increase, beyond the ideal concentration, results in an excess of modified peptide, leading to the formation of spherical particles. Additionally, a thickening of the rod-shaped particles is observed, which subsequently changes the morphology of the particles towards a more spherical shape.

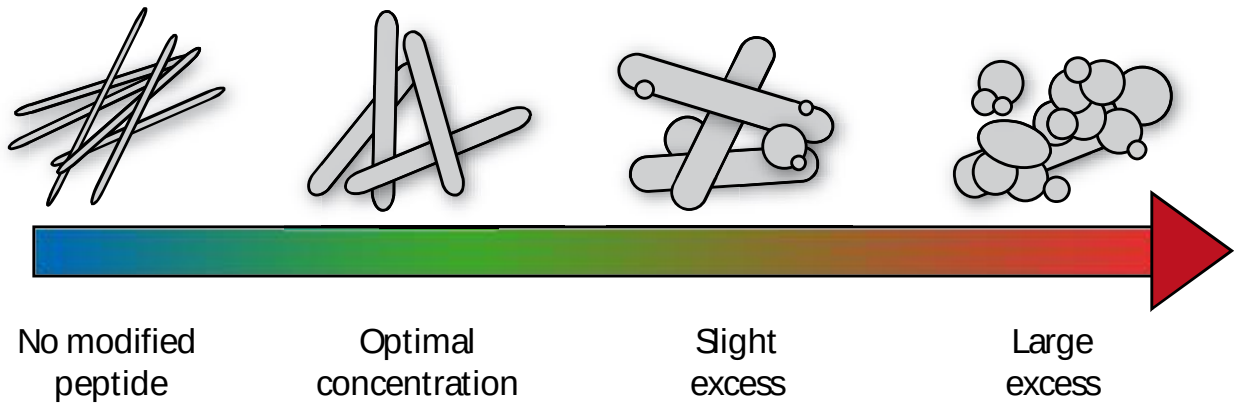

Figure 4-24 Schematic illustration of the morphology of the particles dependent on the concentration of added modified peptide.

4.3.2 Energy-dispersive X-ray spectroscopy (EDX)

To confirm, that the observed particles consisted of peptide and silica, energy-dispersive X-ray spectroscopy was performed. However, only qualitative statements regarding the silica composition can be made by using this method.

The EDX analysis confirmed, that silica is present in all of the investigated samples (Fig. 4-25, 4-26, 4-27). The observed elements originated either from the peptide itself (C, N, O), PBS buffer (P, Cl, Na, K), from the sample stopper (Al, Cu) or the deposited silica (Si). The EDX analysis ensured that all earlier observed particles in the sample resulted from a deposition of silica. The presence of carbon and nitrogen further indicated, that the peptide nanotubes and KRRIL-modified peptides were still within the analyzed sample. Because all particle samples were washed several times to remove remaining traces of silicic acid and peptides, an encapsulation of the nanotubes in a silica shell is reasonable. This strengthens the theory that the modified peptide attaches on the surface of the PNTs and coordinates the deposition of silica on its surface, leading to a protective layer of silica for the PNT.

Furthermore, the EDX analysis confirmed that even the unmodified peptides possess the ability to coordinate the deposition of silica to a certain extend. Yet, it is still unknown if this deposition is induced by the peptide itself or by an auto-condensation of the silicic acid.

No further informations except the presence of silica can be gained from the EDX spectra. To obtain quantitative information on the amount precipitated amount of silica other methods have to be used.

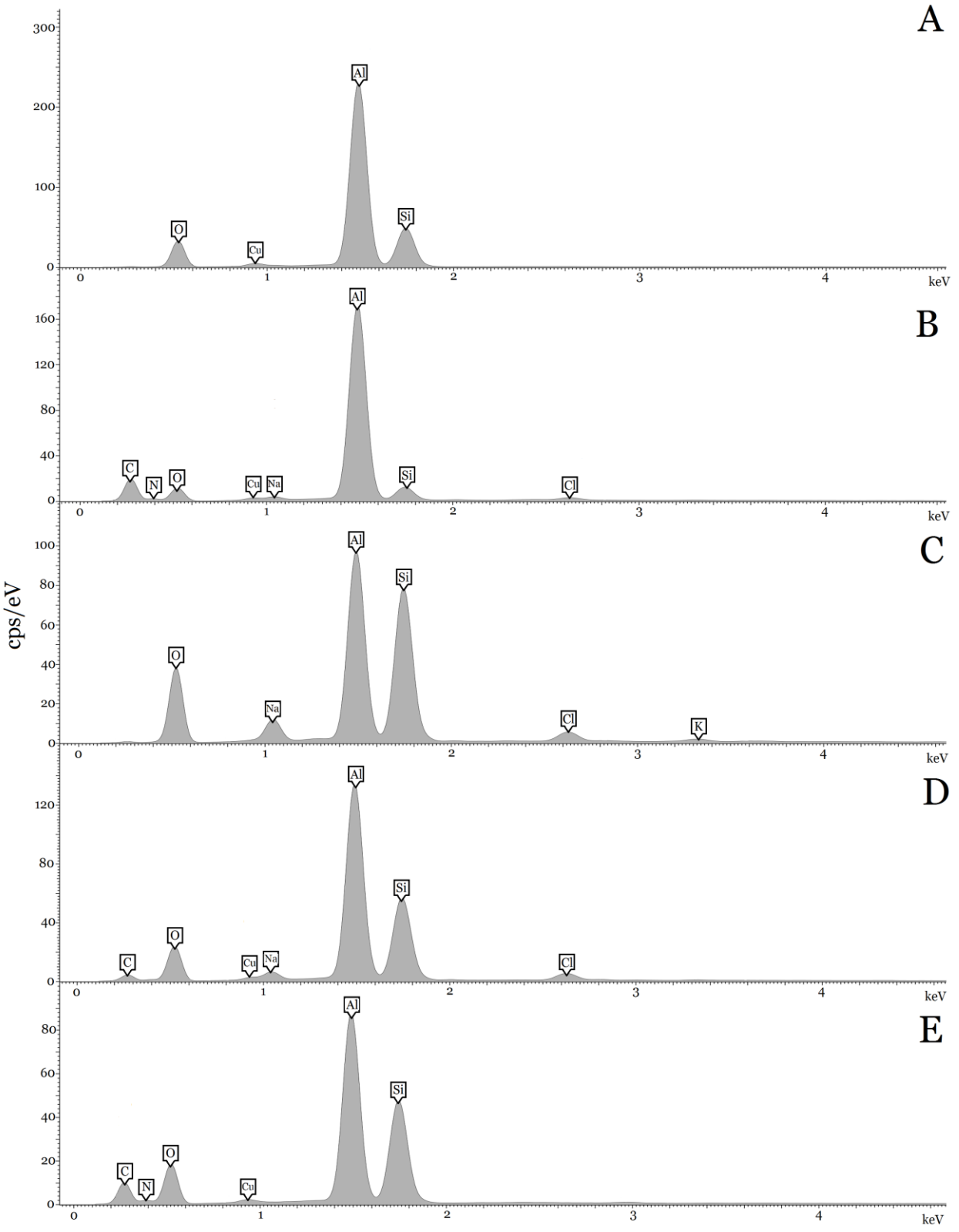

Figure 4-25 EDX analysis of formed particles during *in vitro* silica precipitation. A) 75 µM CC-Hex-T + 25 µM CC-Hex-Mod-1, B) 50 µM CC-Hex-T + 50 µM CC-Hex-Mod-1, C) 25 µM CC-Hex-T + 75 µM CC-Hex-Mod-1, D) 75 µM CC-Pent-T + 25 µM CC-Pent-Mod-1, E) 50 µM CC-Pent-T + 50 µM CC-Pent-Mod-1

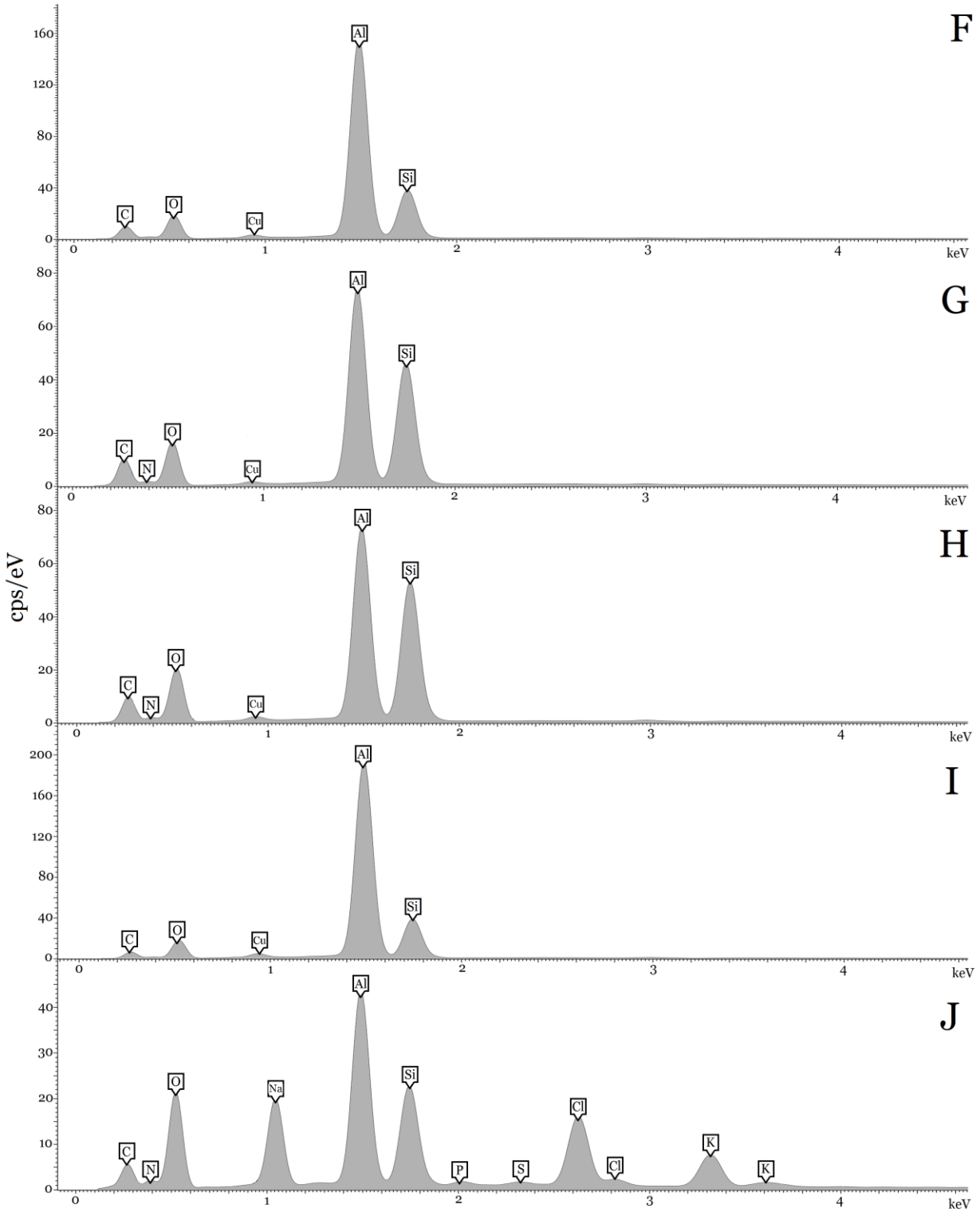

Figure 4-26 EDX analysis of formed particles during *in vitro* silica precipitation. F) 25 µM CC-Pent-T + 75 µM CC-Pent-Mod-1, G) 75 µM CC-Pent-T + 25 µM CC-Pent-Mod-2, H) 50 µM CC-Pent-T + 50 µM CC-Pent-Mod-2, I) 25 µM CC-Pent-T + 75 µM CC-Pent-Mod-2, J) 100 µM CC-Hex-T

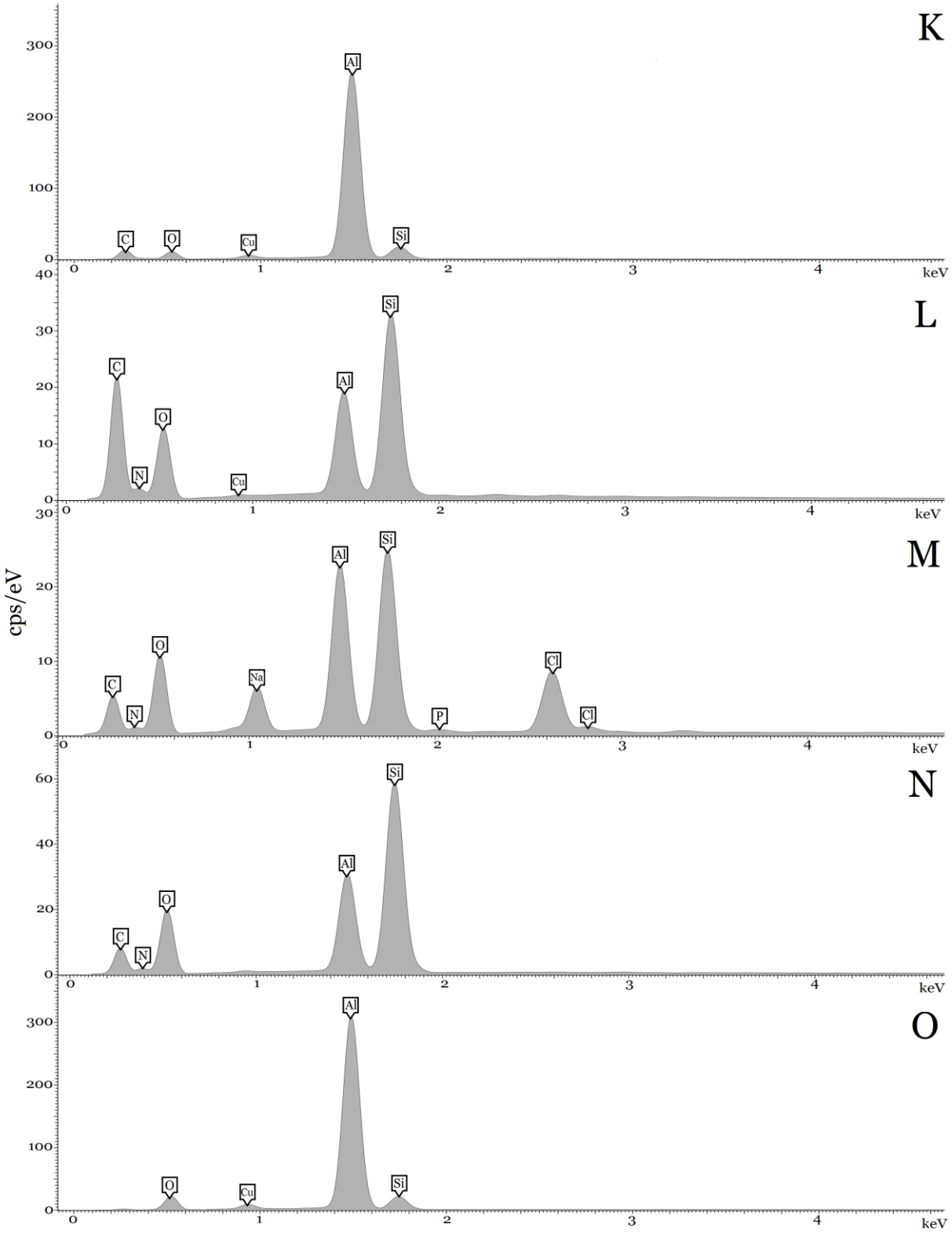

Figure 4-27 EDX analysis of formed particles during *in vitro* silica precipitation. K) 100 µM CC-Hex-Mod-1, L) 100 µM CC-Pent-T, M) 100 µM CC-Pent-Mod-1, N) 100 µM CC-Pent-Mod-2, O) 100 µM KRRIL

4.3.3 Size analysis of precipitated silica particles

To investigate the influence of the deposited silica on the size of the nanotubes, the formed particles of CC-Pent-T and the combined precipitation of CC-Pent-T and CC-Pent-Mod-1 were measured with ImageJ. The calcinated nanotubes of CC-Pent-T displayed an average length of 650 nm and an average diameter of 55 nm (Fig. 4-28). Similar dimensions were observed for the peptide nanotubes, which demonstrates the fineness of the deposited silica layer. Furthermore, it can be concluded, that the silica precipitation does not influence the morphology of the peptide nanotubes, since no further changes in size or shape were observable. Consequently, alterations in the morphology of the particles during the combined precipitation were caused by the modified pentamer with the attached KRRIL sequence.

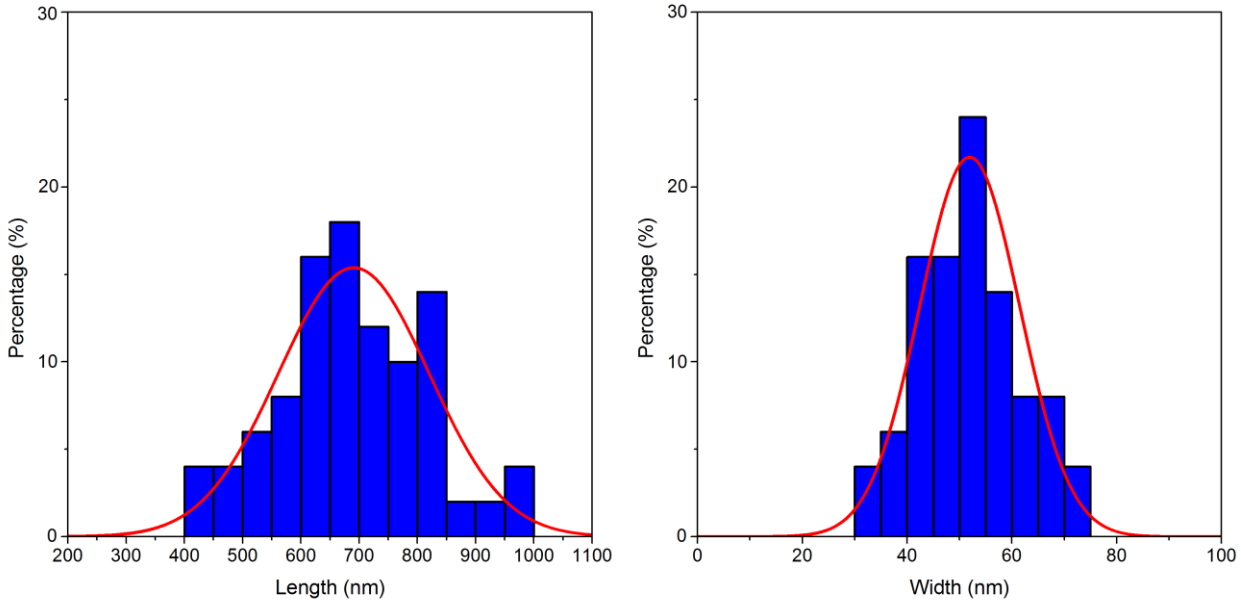

Figure 4-28 Distribution of lengths and widths of precipitated silica particles from CC-Pent-T. Measurements were performed with the corresponding electron micrographs. Bin sizes are 50 nm and 5 nm respectively. A normal distribution curve was fitted over the obtained histogram.

Since the spherical particles were most likely caused solely by CC-Pent-Mod-T, only rod shaped particles were measured to investigate the effect of the KRRIL sequence on the PNTs. For the combined precipitation of CC-Pent-T and CC-Pent-Mod-1 a thickening of the tubes could be observed in all cases (Fig. 4-29). However, the average length of the nanotubes was at all concentrations decreased to around 500 nm. This shortening of the silica particles was most likely caused by the modified pentamer, which interfered with the already assembled nanotubes.

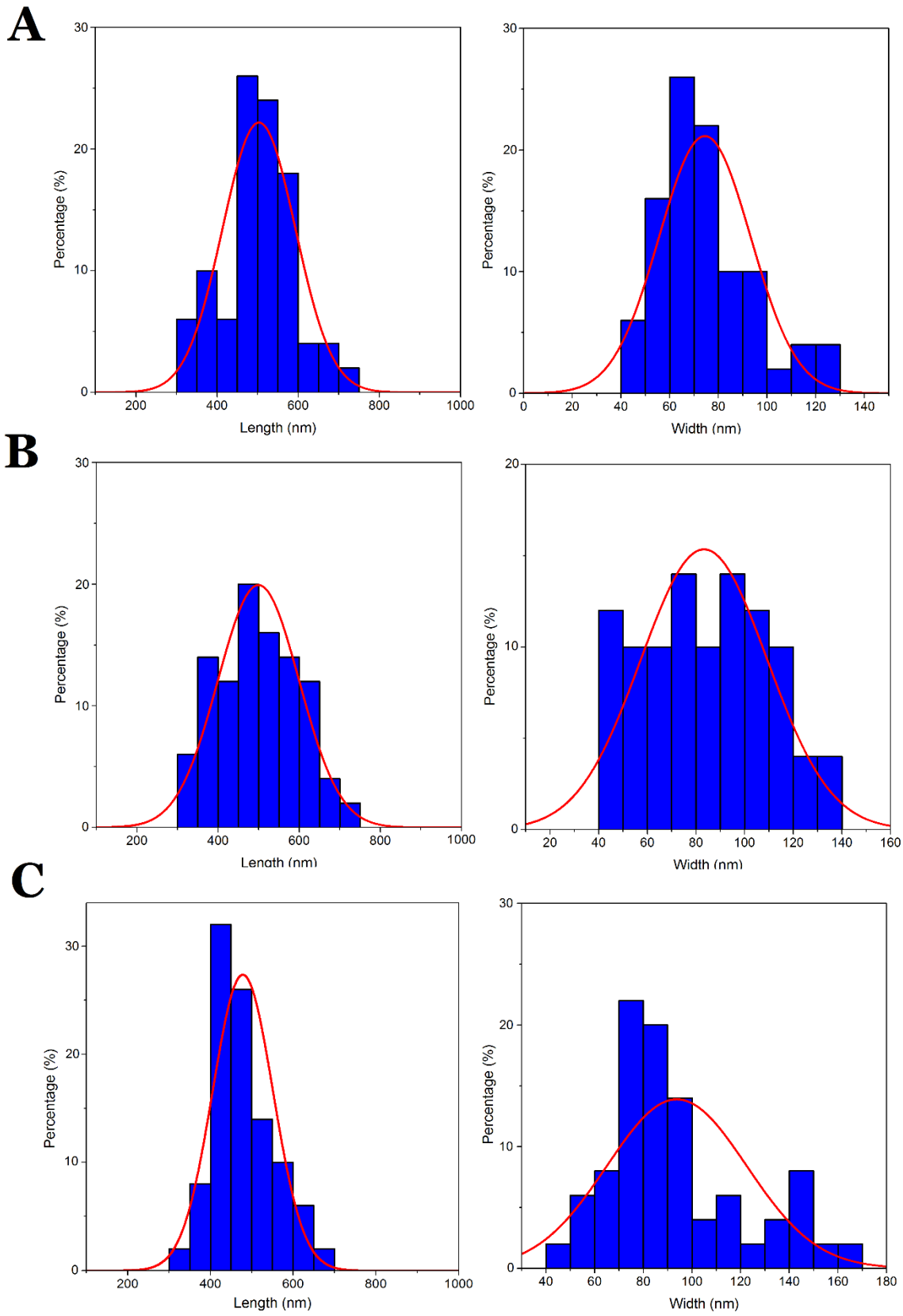

Figure 4-29 Distribution of lengths and widths of silica particles from the combined precipitation of CC-Pent-T and CC-Pent-Mod-1. A) 25 µM CC-Pent-T + 75 µM CC-Pent-Mod-1, B) 75 µM CC-Pent-T + 25 µM CC-Pent-Mod-2, C) 50 µM CC-Pent-T + 50

µM CC-Pent-Mod-2. Measurements were performed with the corresponding electron micrographs. Bin sizes are 50 nm and 5 nm respectively. A normal distribution curve was fitted over the obtained histogram.

The shortening of the PNTs was not further amplified by an increased concentration of CC-Pent-Mod-1. Additionally, the effects of the modified pentamer were clearly evident by the increase in diameter. Even at the lowest concentration of CC-Pent-Mod-1 (25 µM) a shift from 55 nm to 75 nm was observable (Fig. 4-29, A). Therefore, the deposited silica layer had a thickness of around 10 nm. The thickness of the of the layer was further increased to 15 nm (50 µM CC-Pent-Mod-1) (Fig. 4-29, B) and 20 nm (75 µM CC-Pent-Mod-1) (Fig. 4-29, C) respectively. Since the amount of added silicic acid was the same, the increase was only caused by the additional KRRIL sequences. Therefore, the diameter of the silica particles is tunable by the proportion of modified and unmodified pentamer. However, with an increase in concentration also an increase in the inhomogeneity of the diameter was detectable.

4.3.4 Effects of thermal annealing on formed silica particles

The studies of Burgess *et al.* included the thermal unfolding and annealing of the supramolecular assemblies, since they assumed the PNTs are kinetically trapped structures. For CC-Pent-T, they observed a change into broad, sheet-like structures when heated above 40°C and cooled down afterwards.

This behavior of the peptide was further investigated in combination with the deposition of silica, to optimize the formation of silica nanotubes. To evaluate the effect on the PNTs alone, dissolved and incubated CC-Pent-T was heated to 95°C over 180 min and cooled down to 25°C over 20 min afterwards, followed by a silica precipitation. The formed particles displayed analogue characteristics as described by Burgess *et al.* (Fig. 4-30; D, E, F). The silica covered peptides exhibited a shortened and thickened morphology compared to a sample, which did not receive any heat treatment (Fig. 4-30; A, B, C). The particles also appeared to be more clustered and had a less regular surface structure. Since similar changes regarding the shape were observed for the PNTs, the alterations in the morphology of the particles were presumably resulting from the altered superstructure of the nanotubes. The irregular surface of the particle was highly likely caused by free or not properly assembled peptides, since the silica precipitation was immediately performed

after the sample was cooled to room temperature. This further supports the observation, that the peptides take several hours to assemble completely.
Moreover, it can be concluded that the shape and structure of the assembled peptide are the determining factor for the morphology of the particle. The obtained data also indicates, that the addition of the silica does most likely not alter or influence the shape of the assembled peptide nanotubes.

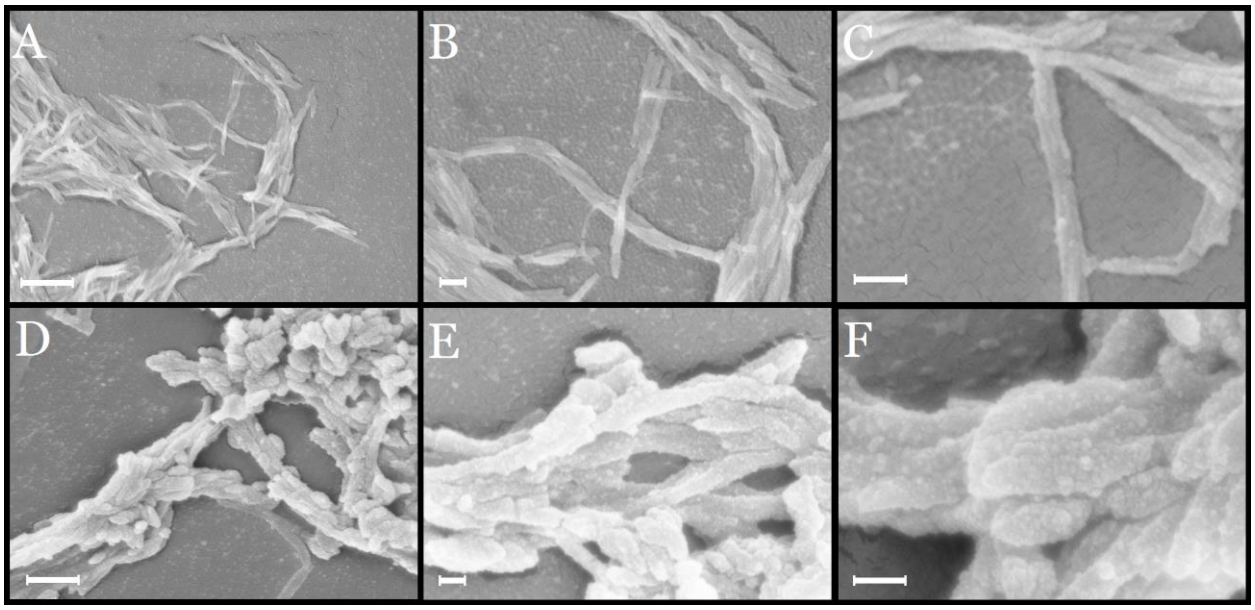

Figure 4-30 Electron micrographs of particles obtained after silica precipitation. CC-Pent-T used without further treatment (A, C, D) and after thermal annealing (D, E, F). Scale bars: 1 µm (A, D), 200 nm (B, E, C, F)

To diminish the particle inhomogeneities when modified and unmodified peptide are combined during the precipitation, thermal annealing was attempted. This could prevent, that clusters of CC-Pent-Mod-1 form spherical particles and ordered assemblies of both peptides are formed. Analogue to before, dissolved CC-Pent-T was incubated for several hours to complete the assembly into nanotubes. Newly dissolved CC-Pent-Mod-1 was added (final concentrations: CC-Pent-T = 75 µM, CC-Pent-Mod-1 = 25 µM), the mixture heated to 95°C and cooled down to 25°C afterwards. The sample was incubated again for 24 h, followed by a silica precipitation.
The observed particles could be divided into two different types (Fig. 4-31). The first particles were similar to the silica structures formed by the nanotubes of CC-Pent-T (Fig. 4-31, B). Those particles most likely originated from peptide nanotubes, which either reassembled into their original form or where the heat treatment had no effect. The

second type was significant shorter and thickened compared to the first ones. Since a similar effect was observed for the nanotubes of CC-Pent-T, it can be assumed that the alterations of the morphology resulted from the thermal annealing. However, a distinct thickening of the particles, caused by the addition of CC-Pent-Mod-1, was not detectable. It was not further studied, if the reduced activity of the modified peptide was the result of heat deactivation or the changed superstructure of the nanotubes. Since the goal of reducing the inhomogeneities in the samples was not accomplished by the thermal annealing, the procedure was not further pursued.

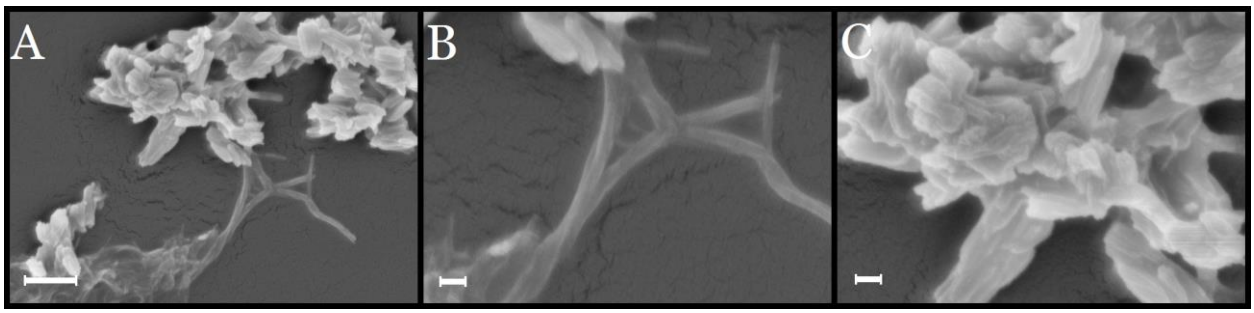

Figure 4-31 Electron micrographs of particles obtained after *in vitro* silica precipitation. Preincubated CC-Pent-T (75 µM) and CC-Pent-Mod-1 (25 µM) were mixed, heated to 95°C and used for the precipitations. Scale bars: 1 µm (A), 200 nm (B, C).

4.3.5 Calcination of silica nano tubes

To effectively use the synthesized silica nanotubes for further applications, remaining organic compounds and water has to be removed beforehand. Both can be achieved by performing a calcination of the nanotubes. During the heat treatment, the encapsulated peptides are thermally decomposed and embedded water evaporates. Since the silica nanotubes were synthesized in small scales, a melting point apparatus was used as first approach for the calcination. Since the particles, which resulted from the combined precipitation of CC-Pent-T (75 µM) and CC-Pent-Mod-1 (25 µM), displayed the most distinct silica nanotubes, the sample was further used for the calcination. A small volume of the sample was heated to 50°C for 15 min to carefully remove the aqueous phase. Afterwards, the sample was heated to 240°C for 1.5 h to get rid of the remaining organic compounds. The treated particles were then examined by ESEM (Fig. 4-32).

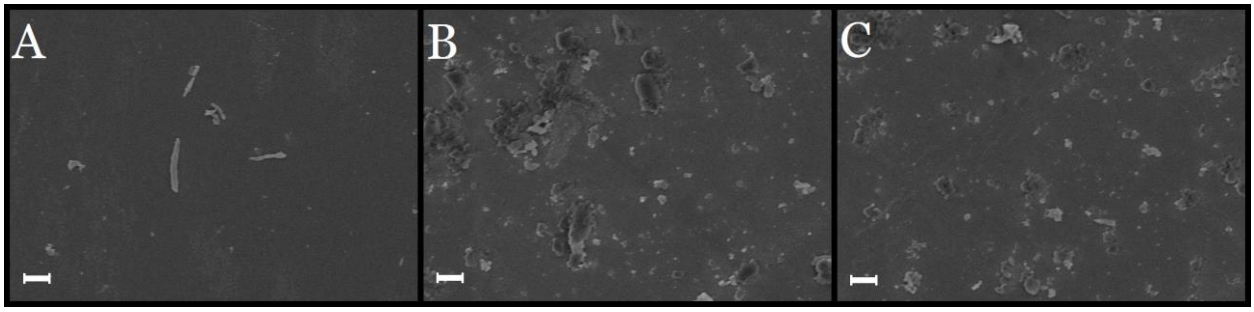

Figure 4-32 Electron micrographs of silica nanotubes after calcination. Particles were obtained from the combined *in vitro* precipitation of CC-Pent-T (75 µM) and CC-Pent-Mod-1 (25 µM) were used. Scale bars: 2 µm (A, B, C).

Only a few intact rod shaped particles were present in the sample (Fig. 4-32, A). The main part of particles lost its original shape and consisted of the scattered and fragmented silica nanotubes. Therefore, the used approach was not successful to calcinate the particles. The damage on the particles indicates, that the silica structures are highly fragile and the calcination has to be done cautiously. There exist several parameters, which can be varied in order to optimize the calcination and prevent a damaging of the nanotubes. Using a flatter gradient, a longer preheating phase or a different device for the calcination would be the first possibilities to experiment on. Furthermore, higher temperatures are needed for an effective removal of the organic components.

4.3.6 Fluorescence microscopy

Little is known about the behavior of the modified coiled-coil peptides in an aqueous environment. Also, the performed ESEM analysis of the functionalized peptides did not reveal any information about their assembly or possible interactions. As a consequence, a derivative of the coiled-coil peptide CC-Pent-T was synthesized with the fluorophore Cy5 attached. The linkage between the peptide and Cy5 is analogue to the attachment of the KRRIL sequence. Having a fluorophore coupled to the peptide allows the examination of the peptide in an aqueous environment by fluorescence microscopy. Furthermore, no direct intrusion in the peptide sample is needed using this approach.

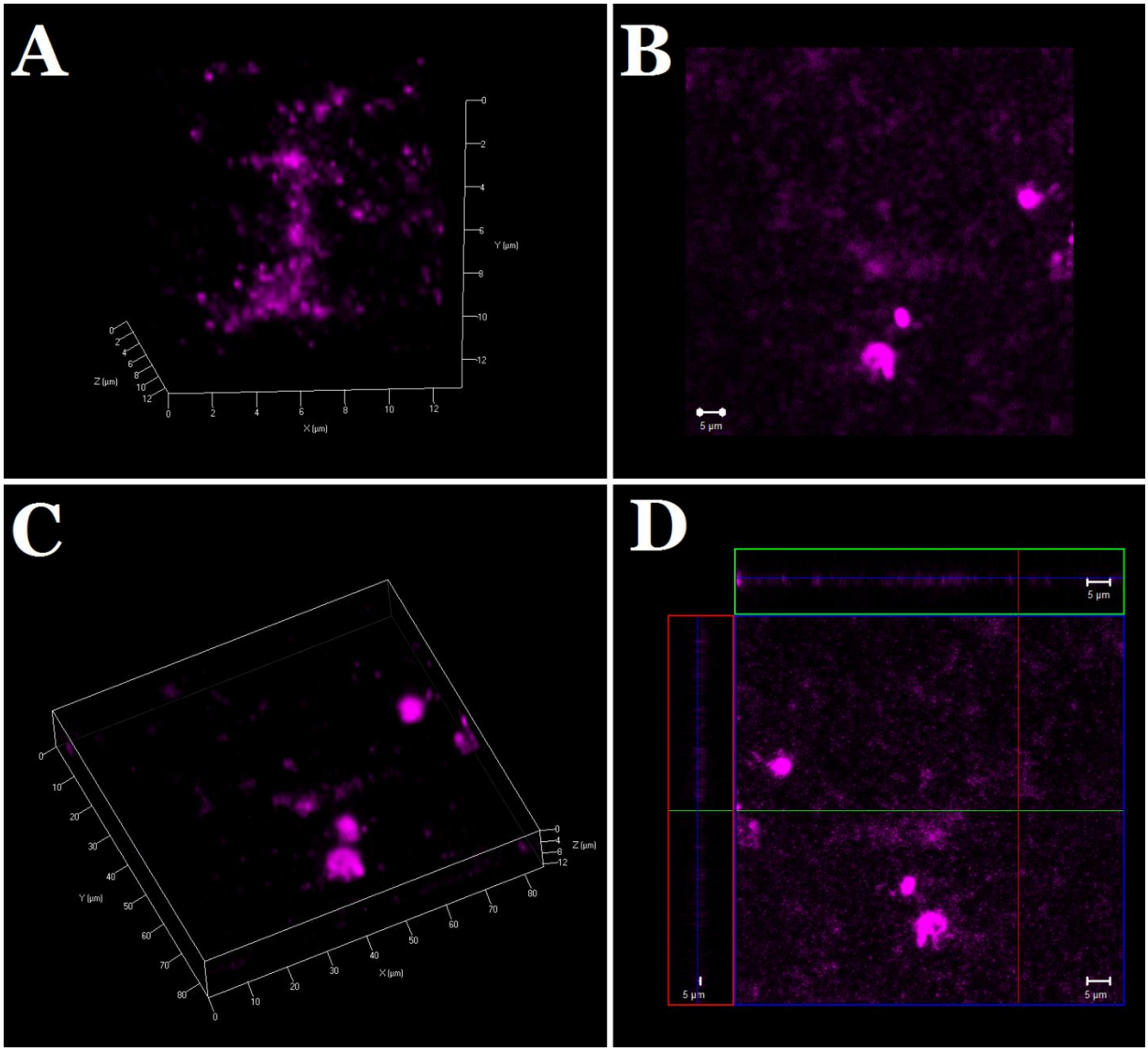

Figure 4-33 Obtained images from the fluorescence microscopy of CC-Pent-Cy5 at a concentration of 10 µM. Different visualization methods were used to study the interaction of the peptide (A-D). Scale bars: 5 µm.

Using fluorescence microscopy, no fiber like structures could be detected with the used setup and visualization methods (Fig. 4-33). The observed fluorescent structures originated most likely from aggregated peptides, which did not assemble correctly. Since Cy5 is a hydrophobic modification of the coiled-coil peptide, an interference with the assembly into α-helical barrels is possible. These results would be in line with the attachment of the KRRIL motive, which also interferes with the interactions of the peptides. Therefore, analogous to the KRRIL modification, a different approach to visualize fluorescent PNTs has to be used.

5 Conclusion and outlook

The primary goal to obtain silica nanotubes with a peptide, which combines two building blocks, could not be achieved. An assembly into peptide nanotubes could not be observed for all the KRRIL-functionalized peptides. Furthermore, only spherical or heterogeneous silica nano particles could be obtained during an *in vitro* silica precipitation. From the performed experiments, including CD-spectrometry and DPH intercalation, it can be assumed, that the attachment of the KRRIL tag does disturb the assembly of the coiled-coil peptides. However, it does not inhibit the ability of the silaffin derivate to deposit silica. The modification with Cy5 revealed an analogous behaviour, which resulted in the aggregation of the peptides and no observable nanotubes.

To overcome the inhibited assembly of the peptides, a combined precipitation with preassembled nanotubes and the functionalized pentamer was performed. This should result in PNTs, which are surrounded by a sheath of KRRIL modified peptide. Using this method, the goal of silica nanotubes could be achieved. The precipitated particles displayed a layer of silica deposited on the surface of the peptides. Furthermore, the thickness of the layer could be controlled by the concentration of the peptides. However, an increased amount of the modified peptide results in an inhomogeneity of silica nanotubes and an increase in spherical particles.

It could be demonstrated that it is possible to obtain silica nanotubes by using two peptides, which consist of a coiled-coil and silaffin building block. The KRRIL sequence actively precipitates silica on the surface of the nanotubes by a coordinated deposition. However, since the KRRIL sequence disturbs the assembly of the PNTs, methods to bypass this effect have to be found. Covalently linking the coiled-coil peptides could be a possible solution, because no charge dependent assembly would be necessary. Furthermore, spherical particles, which result from modified peptide, which did not attach to the PNTs, would be eliminated. By using a proper method to calcinate the silica nanotubes, the particles could be used for various applications. Since PNTs can be synthesized with broad variety of lengths and widths, a convenient method to produce specifically tailored silica nanotubes has been found. Furthermore, the biomimetically formation of the particles allows a fast synthesis under mild reaction conditions.

6 Abbreviations

°C	Degree Celsius
µL	Microliter
µM	Micromolar
µm	Micrometer
A, Ala	Alanine
aa	Amino acid
ACN	Acetonitrile
Al	Aliminium
Boc	Tert-butyloxycarbonyl
C	Carbon
CD	Circular dichroism
cDNA	Complementary DNA
Cl	Chlorine
cm	Centimeter
cps	Counts per second
Cu	Copper
Da	Dalton
DCM	Dichloromethane
ddH_2O	Double distilled water
DIC	N,N′-diisopropylcarbodiimide
DIEA	N,N-diisopropylethylamine
DMF	N,N-dimethylformamide
DPH	1,6-diphenyl-1,3,5-hexatrien
E, Glu	Glutamic acid
EDT	1,2-ethanedithiol
EDX	Energy-dispersive X-ray spectroscopy
eq.	Equivalents
ESI-MS	Electrospray ionization mass spectrometry
et al.	Et alii (and others)
Et_2O	Diethylether
eV	Electronvolt
Fig.	Figure

Fmoc	Fluorenylmethoxycarbonyl
g	Gram
Gt	Gigatonne
h	Hour
HBTU	2-(1H-benzotriazol-1-yl)-1,1,3,3-tetramethyluronium hexafluorophosphate
HPLC	High pressure liquid chromatography
I, Ile	Isoleucine
K	Potassium
K, Lys	Lysine
kDA	Kilodalton
kV	Kilovolt
L, Leu	Leucine
LCPA	Long chain polyamines
M	Molar
mg	Milligram
min	Minute
mL	Milliliter
mm	Millimeter
mmol	Millimol
MS	Mass spectrometry
MSN	Mesoporous silica nanoparticle
Mtt	4-methyltrityl
N	Nitrogen
Na	Sodium
nm	Nanometer
NMR	Nuclear magnetic resonance
O	Oxygen
P	Phosphorus
PBS	Phosphate buffered saline
PNT	Peptide nanotube
PV	Peptide velcro
Q, Gln	Glutamine
R, Arg	Arginine

RP-HPLC	Reversed phase high pressure liquid chromatography
s	Second
SDS-Page	Sodium dodecyl sulfate polyacrylamide gel electrophoresis
SDV	Silica deposition vesicles
SEM	Scanning electron microscope
Si	Silicon
SIT	Silicic acid transporter protein
SPPS	Solid phase peptide synthesis
TEM	Transmission electron microscope
TFA	Trifluoroacetic acid
TIPS	Triisopropylsilane
TMOS	Tetramethoxysilane
UV	Ultraviolett
Vis	Visible
vol.	Volume

7 Literature

[1] P. R. Odgren, “Phylogenetic Occurrence of Coiled Coil Proteins: Implications for Tissue Structure in Metazoa via a Coiled Coil Tissue Matrix,” *Proteins: Structure, Function, and Genetics*, vol. 24, pp. 467-484, 1996.

[2] F. H. C. Crick, “The Packing of a-Helices: Simple Coiled-Coils,” *Acta Crystallographica*, vol. 6, pp. 689-697, 14 March 1953.

[3] J. Liu, "A seven-helix coiled coil," *Proceedings of the National Academy of Sciences of the United States of America*, vol. 103, no. 42, pp. 15457-15462, October 2006.

[4] L. Pauling, "Compound Helical Configurations of Polypeptide Chains: Structure of Proteins of the α-Keratin Type," *Nature*, pp. 59-61, January 1953.

[5] C. Vinson, "Scissors-grip model for DNA recognition by a family of leucine zipper proteins," *Science*, vol. 246, no. 4932, pp. 911-916, 17 November 1989.

[6] D. C. Chan, "HIV Entry and Its Inhibition," *Cell*, vol. 93, no. 5, pp. 681-684, 29 May 1998.

[7] B. Tripet, "Engineering a de novo-designed coiled-coil heterodimerization domain for the rapid detection, purification and characterization of recombinantly expressed peptides and proteins," *Protein engineering*, vol. 9, no. 11, pp. 1029-1042, 1996.

[8] W. D. Kohn, "α-Helical Protein Assembly Motifs," *The Journal of Biological Chemistry*, vol. 272, no. 5, pp. 2583-2586, 31 January 1997.

[9] E. O'Shea, "Peptide 'Velcro': design of a heterodimeric coiled coil," *Current biology*, vol. 3, no. 10, pp. 658-667, 1 October 1993.

[10] E. O'Shea, "X-ray structure of the GCN4 leucine zipper, a two-stranded, parallel coiled coil," *Science*, vol. 254, no. 5031, pp. 539-544, 25 October 1991.

[11] P. B. Harbury, "A switch between two-, three-, and four-stranded coiled coils in GCN4 leucine zipper mutants," *Science*, vol. 262, no. 5138, pp. 1401-1407, 26 November 1993.

[12] J. M. Mason, "Coiled Coil Domains: Stability, Specificity, and Biological Implications," *ChemBioChem*, vol. 5, no. 2, pp. 170-176, 29 January 2004.

[13] Y. Tang, "Biosynthesis of a Highly Stable Coiled-Coil Protein Containing Hexafluoroleucine in an Engineered Bacterial Host," *Journal of the American Chemical Society*, vol. 44, pp. 11089-11090, 11 October 2001.

[14] T. J. Graddis, "Controlled formation of model homo- and heterodimer coiled coil

polypeptides," *Biochemistry*, vol. 32, no. 47, pp. 12664-12671, 30 November 1993.

[15] W. D. Kohn, "Protein destabilization by electrostatic repulsions in the two-stranded alpha-helical coiled-coil/leucine zipper," *Protein Science*, vol. 4, no. 2, pp. 237-250, February 1995.

[16] K. M. Arndt, "Comparison of in vivo selection and rational design of heterodimeric coiled coils," *Structure*, vol. 10, no. 9, pp. 1235-1248, September 2002.

[17] V. Dinca, "Directed Three-Dimensional Patterning of Self-Assembled Peptide Fibrils," *Nano Letters*, vol. 8, no. 2, pp. 538-543, March 2008.

[18] L. Adler-Abramovich, "Thermal and chemical stability of diphenylalanine peptide nanotubes: implications for nanotechnological applications," *Langmuir*, vol. 22, no. 3, pp. 1313-1320, 31 January 2006.

[19] S. Vauthey, "Molecular self-assembly of surfactant-like peptides to form nanotubes and nanovesicles," *Proceedings of the National Academy of Sciences of the United States of America*, vol. 99, no. 8, pp. 5355-5360, 16 April 2002.

[20] M. Amorín, "New Cyclic Peptide Assemblies with Hydrophobic Cavities: The Structural and Thermodynamic Basis of a New Class of Peptide Nanotubes," *Journal of the American Chemical Society*, vol. 125, no. 10, pp. 2844-2845, 19 February 2003.

[21] E. H. Engelman, "Structural Plasticity of Helical Nanotubes Based on Coiled-Coil Assemblies," *Structure*, vol. 23, no. 2, pp. 280-289, 3 February 2015.

[22] F. Thomas, "Controlling the Assembly of Coiled-Coil Peptide Nanotubes," *Angewandte Chemie (International ed. in English)*, vol. 55, no. 3, pp. 987-991, 18 January 2016.

[23] N. C. Burgess, "Modular Design of Self-Assembling Peptide-Based Nanotubes," *Journal of the American Chemical Society*, vol. 137, no. 33, pp. 10554-10562, 28 July 2015.

[24] M. Yemini, "Peptide Nanotube-Modified Electrodes for Enzyme–Biosensor Applications," *Analytical Chemistry*, vol. 77, no. 16, 30 June 2005.

[25] J. V. Veeril, "Tailored Carbon Nanotubes for Tissue Engineering Applications," *Biotechnology progress*, vol. 25, no. 3, pp. 709-721, 11 December 2009.

[26] S. Alam, "Short peptide based nanotubes capable of effective curcumin delivery for treating drug resistant malaria," *Journal of nanobiotechnology*, vol. 14, no. 26, 11 December 016.

[27] L. Adler-Abramovich, "Self-assembled arrays of peptide nanotubes by vapour deposition," *Nature nanotechnology*, vol. 4, pp. 849-854, 18 October 2009.

[28] J. Sanchis, "Cyclic Peptide Nanotubes for Drug Delivery," 2016.

[29] J. J. Castillo, "Detection of cancer cells using a peptide nanotube–folic acid modified graphene electrode," *Analyst*, vol. 138, pp. 1026-1031, 26 October 2012.

[30] R. I. MacCuspie, "Virus assay using antibody-functionalized peptide nanotubes," *Soft Matter*, vol. 4, pp. 833-839, 22 February 2008.

[31] B. Bailleul, "Energetic coupling between plastids and mitochondria drives CO2 assimilation in diatoms," *Nature*, vol. 524, pp. 366-369, 20 August 2015.

[32] T. A. Norton, "Algal biodiversity," *Phycologia*, vol. 35, no. 4, pp. 308-326, July 1996.

[33] F. Round, The Diatoms: Biology and Morphology if the Genera, Cambridge: *Cambridge University Press*, 1990.

[34] Y. D. Amo, "The chemical form of dissolved Si taken up by marine diatoms," pp. 1162-1170, 1999.

[35] M. Hildebrand, "A gene family of silicon transporters," *Nature*, vol. 385, no. 6618, pp. 688-689, 20 February 1997.

[36] T. L. Simpson, Silicon and Siliceous Structures in Biological Systems, New York: *Springer-Verlag*, 1981.

[37] N. Kröger, "Species-specific polyamines from diatoms control silica morphology," *Proceedings of the National Academy of Sciences of the United States of America*, vol. 97, no. 26, pp. 14133-14138, 19 December 2000.

[38] N. Kröger, "Polycationic peptides from diatom biosilica that direct silica nanosphere formation," *Science*, vol. 286, no. 5442, pp. 1129-1132, 5 November 1999.

[39] N. Kröger, "Self-Assembly of Highly Phosphorylated Silaffins and Their Function in Biosilica Morphogenesis," *Science*, vol. 298, no. 5593, pp. 584-586, 18 October 2002.

[40] N. Kröger, "Silica-precipitating Peptides from Diatoms," *The Journal of Biological Chemistry*, vol. 276, no. 28, pp. 26066-26070, 13 July 2001.

[41] C. Lechner, Functional analysis and biotechnological applications of silaffin peptides, München, 2013.

[42] Genicap, „Digital Diatoms, “. Available: http://genicap.com/category/genicapart/digital-diatoms/.

[43] M. Vallet-Regì, "Mesoporous Materials for Drug Delivery," *Angewandte Chemie (International ed. in English)*, vol. 46, no. 40, pp. 7548-7558, 13 September 2007.

[44] B. Trewyn, "Biocompatible mesoporous silica nanoparticles with different morphologies for animal cell membrane penetration," *Chemical Engineering Journal*, vol. 137, no. 1, pp. 23-29, 15 March 2008.

[45] R. Mortera, "Cell-induced intracellular controlled release of membrane impermeable cysteine from a mesoporous silica nanoparticle-based drug delivery system," *Chemical Communications*, vol. 22, pp. 3219-3221, 07 May 2009.

[46] C. Charnay, "Inclusion of ibuprofen in mesoporous templated silica: drug loading and release property," *European Journal of Pharmaceutics and Biopharmaceutics*, vol. 57, no. 3, pp. 533-540, May 2004.

[47] A. Nieto, "Surface Electrochemistry of Mesoporous Silicas as a Key Factor in the Design of Tailored Delivery Devices," *Langmuir*, vol. 26, no. 7, pp. 5038-5049, 2010.

[48] I. Slowing, "Mesoporous silica nanoparticles for intracellular delivery of membrane-impermeable proteins," *Journal of the American Chemical Society*, vol. 129, no. 28, pp. 8845-8849, 18 July 2007.

[49] J. Rosenholm, "Targeting of porous hybrid silica nanoparticles to cancer cells," *ACS Nano*, vol. 3, no. 1, pp. 197-206, 27 January 2009.

[50] C.-P. Tsai, "Monoclonal antibody-functionalized mesoporous silica nanoparticles (MSN) for selective targeting breast cancer cells," *Journal of Materials Chemistry*,
vol. 19, pp. 5737-5743, 24 June 2009.

[51] D. Shao, "Janus "nano-bullets" for magnetic targeting liver cancer chemotherapy," *Biomaterials*, vol. 200, pp. 118-133, Spetember 2016.

[52] Y. Wei, "Simultaneous Immobilization of Horseradish Peroxidase and Glucose Oxidase in Mesoporous Sol–Gel Host Materials," *ChemPhysChem*, vol. 3, no. 9, pp. 802-808, 16 September 2002.

[53] Z. Dai, "Direct electron transfer and enzymatic activity of hemoglobin in a hexagonal mesoporous silica matrix," *Biosensors & Bioelectronics*, vol. 19, no. 8, pp. 861-867, 2004.

[54] T. Delclos, "Individualized Silica Nanohelices and Nanotubes: Tuning Inorganic Nanostructures Using Lipidic Self-Assemblies," *Nano Letters*, vol. 8, no. 7, pp. 1929-1935, July 2008.